



Transfer of industrial contaminants from the inner to the outer region of Sepetiba Bay (SE Brazil) by dredge spoil dumping activities: a temporal record

Murilo Barros Saibro¹ · Maria Virgínia Alves Martins^{1,2} · Josefa Varela Guerra³ · Rubens Cesar Lopes Figueira⁴ · Felipe de Castro Figueiredo Simões³ · Tatiana Pinheiro Dadalto⁵ · Tailisi Hoppe Trevizani⁴ · Paulo Alves de Lima Ferreira⁴ · Cleverson Guizan Silva⁶ · Antônio Tadeu dos Reis³ · Denise Terroso² · Layla Cristine da Silva¹ · Sergio Bergamaschi¹ · Fernando Rocha² · Monica Heilbron¹

Received: 20 February 2023 / Accepted: 24 October 2023 / Published online: 8 November 2023
© The Author(s) 2023

Abstract

A multiproxy approach involving grain size, geophysical (resistivity, magnetic susceptibility, and P-wave velocity), mineralogical (XRD), and geochemical (elemental, stable isotopes) data has been applied to core SP9 (128 cm long) to reconstruct natural and anthropogenic changes since ≈ 1850 AD (anno domine) (dating by ^{210}Pb and ^{137}Cs methods) in a distal region of Sepetiba Bay (SB), Rio de Janeiro State (SE Brazil). The analyzed core is a fine-grained sedimentary sequence (except its upper 20 cm). It comprises detrital particles derived from felsic and intermediate source rocks, as suggested by the fields defined by the biplot Zr vs TiO_2 and the $\text{Al}_2\text{O}_3/\text{TiO}_2$ ratios. Despite the increase in particle size at the top of the core, there was a progressive increase in the organic matter and potentially toxic elements (PTEs) contents and nutrients such as N and P. The geophysical data allowed us to identify the presence of subsurface (biogenic) gas, which suggests the occurrence of eutrophication processes in the study area despite its location in the outer region of the bay. Core SP9 records cyclical changes over the last ≈ 170 years in the mineralogical and elemental composition of the sediments and type of organic matter supplied to the bottom. These changes are associated with phases of more significant oceanic influence, salinity variations in the study area, and greater or lesser oxygen depletion in the sediment. These changes may have resulted from climatic oscillations or variations in the configuration and extension of the Ponta da Pombeba spit. The extent of this structure and the anthropic activities have contributed to the contamination of this area since 1975 AD. However, statistical analyses (Pearson correlations and principal components analysis) suggest that the transport and accumulation of PTEs (mainly Cd and Zn) did not strictly follow the general pattern of sedimentary dynamics prevailing in the studied area. Results indicate that this area became strongly polluted by Cd and Zn and with high ecological risk due to dredging and spoil disposal activities at sites close to the study area. It is noted that the environmental degradation reached higher levels here than in areas close to the primary source of the metals, the disabled Ingá Mercantil Company, in Madeira Island. This work demonstrates the temporal effect of dredge disposal activities in a distal region of Sepetiba Bay for the first time. It is a strong indicator that dredged spoil areas must be selected carefully, since healthy areas can become degraded due to the dumping of polluted waste.

Keywords Dredging · Spoil disposal · Pollution · Sediment provenance · Geochemical proxies · Geophysical data · Temporal record

Introduction

The evolution of coastal systems constitutes one of the major current concerns of humanity (Perez Filho and Rubira 2019; Souza et al. 2020). It has been influenced by multiple factors,

such as changes in continent–ocean interaction, shoreline stability, sediment dynamics, human activities, environmental quality, and the integrity of coastal ecosystems (Fernandez et al. 2017; Lämmle et al. 2022). In this context, it is necessary to understand the current state of coastal systems and their history over diverse time scales.

In the last decades, the uncontrolled advance of urbanization, anthropic interventions, and the expansion of industrial

Extended author information available on the last page of the article

activities in coastal regions have left signs of disturbance of the natural sediment dynamics (Castelo et al. 2021a, b; Gabriel et al. 2021), causing, among other, significant morphological changes and increased eutrophication and pollution (Tian et al. 2019; Birk et al. 2020; Lürling and Mucci 2020; Wang et al. 2021). The study of sediment cores collected in coastal systems has allowed the identification of the overtime impact of anthropic actions (Krippner et al. 2016; Aguiar et al. 2021) and the assessment of the magnitude of their impacts (Silva et al. 2022a, b).

In highly urbanized harbor regions where many industries are located, dredging activities to provide access to the port for sizeable sea-going cargo vessels and disposal of dredged materials have been causing increased problems, which are a significant concern for coastal systems. The adverse effects of the disposal of dredged waste at sea—such as interference with fishing activities or contamination of ecosystems—have been increasingly recognized. These activities have degraded the environmental quality of coastal marine ecosystems and have negatively interfered with fishing activities. The Convention on the Prevention of Marine Pollution by Dumping of Wastes and Other Matter 1972, known as the London Convention, attempted to solve the problem. International agreements such as the Oslo Convention, the United Nations Convention on the Law of the Sea, and the OSPAR guidelines were established to protect the marine environment from these human activities. These regulations describe good practices to protect the environment from the management of dredged material. In many countries, authorities started to select disposal areas where the negative impact of these activities was minimized. Several regulations have been established in Brazil to control dredging activities and protect coastal systems, such as CONAMA (2004, 2012). Even so, there are several highly anthropized Brazilian coastal systems where critical port activities take place, such as, among others, Todos os Santos Bay (Brito et al. 2012), Santos Bay (Netto et al. 2022), Guanabara Bay (Vilela et al. 2014; Potratz et al. 2019; Alves Martins et al. 2020; Nunes et al. 2023), Paranaguá Bay (Vieira et al. 2021), and Sepetiba Bay (Araújo et al. 2017a, b; Morales et al. 2019a, b; Souza et al. 2021; Castelo et al. 2021a, b; Silva et al. 2022a, b).

The study area of this paper is located in Sepetiba Bay, a highly anthropized coastal system where dredging, extraction, and spoil disposal activities constantly occur (Wasserman et al. 2013). Previous investigations conducted in Sepetiba Bay have sought to identify the consequences of human activities in recent decades (Nascimento et al. 2016; Araújo et al. 2017a, b; Alves Martins et al. 2019; Castelo et al. 2021a, b; Silva et al. 2022a, b), including issues related to changes in the rate and source of pollutants (Ferreira and Moreira 2015; Rodrigues et al. 2020). However, we need to be aware of studies that have tried to discriminate the temporal influence of natural processes and dredge spoil dumping

activities on the transfer of industrial contaminants from the inner to the outer region of Sepetiba Bay (SE Brazil). The analyzed area is located near Marambaia Barrier Island and Ponta da Pombeba spit and sites used in the past to dispose of dredged materials. The work applies a multiproxy methodology (including geophysical, textural, geochemical, and mineralogical data) along core SP9 (Fig. 1). In it, questions related to sediment dynamics, sediment provenance, weathering, paleosalinity, paleoredox conditions, climate oscillations, and anthropogenic influence were investigated. Selected data obtained at core SP9 were compared with that of previously studied cores to contextualize better the results acquired there.

Study area

The study area is on the present configuration included in Sepetiba Bay is a coastal lagoon located 60 km west of the city of Rio de Janeiro (SE Brazil), between latitudes 22°54' and 23°04' S and longitudes 43°34' and 44°10' W (Fig. 1). The bay is an ellipsoidal shaped coastal water body bounded by the Serra do Mar rock massif to the north, the Guaratiba tidal plain to the east, a series of islands with migmatitic rocks to the west (e.g., Itacuruçá, Jaguanum and Guaíba islands) and the ~43 km long Marambaia Barrier Island to the south (Dantas 2000). The Marambaia barrier island was formed following the sea level rising during the post-latest glacial period (Friederichs et al. 2013; Reis et al. 2013, 2020; Dadalto et al. 2021). It plays a significant role in altering the sedimentary and oceanographic dynamics within Sepetiba Bay.

The Sepetiba Bay watershed comprises diverse rock types and terrains from Precambrian to Quaternary units (Fig. 2). The rock units are included in the Paraíba do Sul Terrane, a geotectonic unit with many lithologies, being composed mainly of metamorphic rocks, such as migmatites, gneisses, and gneiss-granitoids. The Rio Negro Complex is a lithodemic unit which comprises granites, tonalites and granodiorites of the Neoproterozoic (Tupinambá et al. 2000; Heilbron and Machado 2003; Misumi et al. 2014).

According to the Köppen–Geiger classification, the Sepetiba Bay region is under the influence of the Tropical Af Zone, i.e., it is characterized by hot and humid conditions, without the presence of dry seasons and with a small temperature range (Kottek et al. 2006; Alvares et al. 2013). The climate is largely controlled by the South Atlantic Convergence Zone (SACZ; Carvalho et al. 2003), secondarily by cold fronts and, locally, by orographic effects related to the proximity of Serra do Mar escarpments to the ocean (Cunha et al. 2006). Due to the relief and the proximity to the ocean, the wind presents, as a first predominance, the south (S) and west–southwest (OSO) quadrants and as

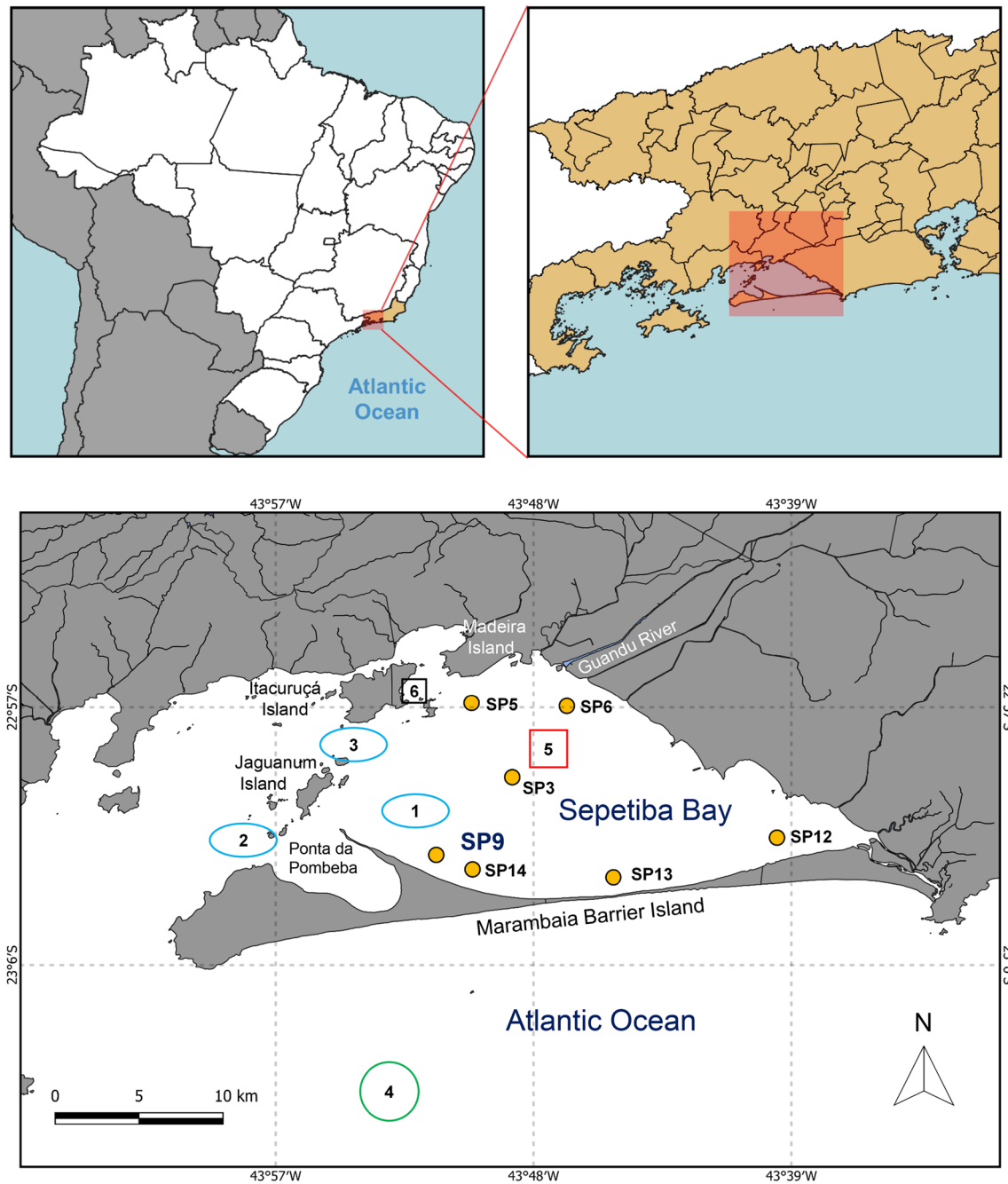


Fig. 1 Location map of Sepetiba Bay (SE Brazil; Rio de Janeiro State) and core SP9 studied in this work. P-wave velocity data obtained in cores SP12, SP13, and SP14, collected near Marambaia Barrier Island, were also compared with those acquired in core SP9 as well as some geochemical data obtained in cores SP3 (Castelo et al. 2021a, b), SP5 (Silva et al. 2022a, b) and SP6 (Alves Martins et al. 2019). The map shows the disposal areas for dredging material in Sepetiba Bay (according to Rodrigues et al. 2020). Blue ellipses

1, 2, and 3 are areas used by CDRJ (Companhia Docas do Rio de Janeiro), green circle 4 is the external disposal area which is currently used for the deposition of dredged; red square 5 is the confined disposal facility (CDF) used by ThyssenKrupp Companhia Siderúrgica do Atlântico—Rio de Janeiro/RJ (CSA) and; black square 6 is the CDF used by Porto Sudeste. Geographic Coordinate System, datum SIRGAS 2000, IBGE, INPE, Natural Earth Data

a second predominance, the north–northeast (NNE) and east–northeast (ENE) quadrants. The Santa Cruz Air Force Base meteorological station indicates that the percentage of calm winds (19.4%) was considerably lower than that of

winds with speeds in the range of 1.5–5.0 m/s (67.7%) in the period between 1981 and 1989 (SEMADS 2001).

Water circulation in the bay is controlled by tides (Leal Neto et al. 2006; Kjerfve et al. 2021) and wind. Tidal data

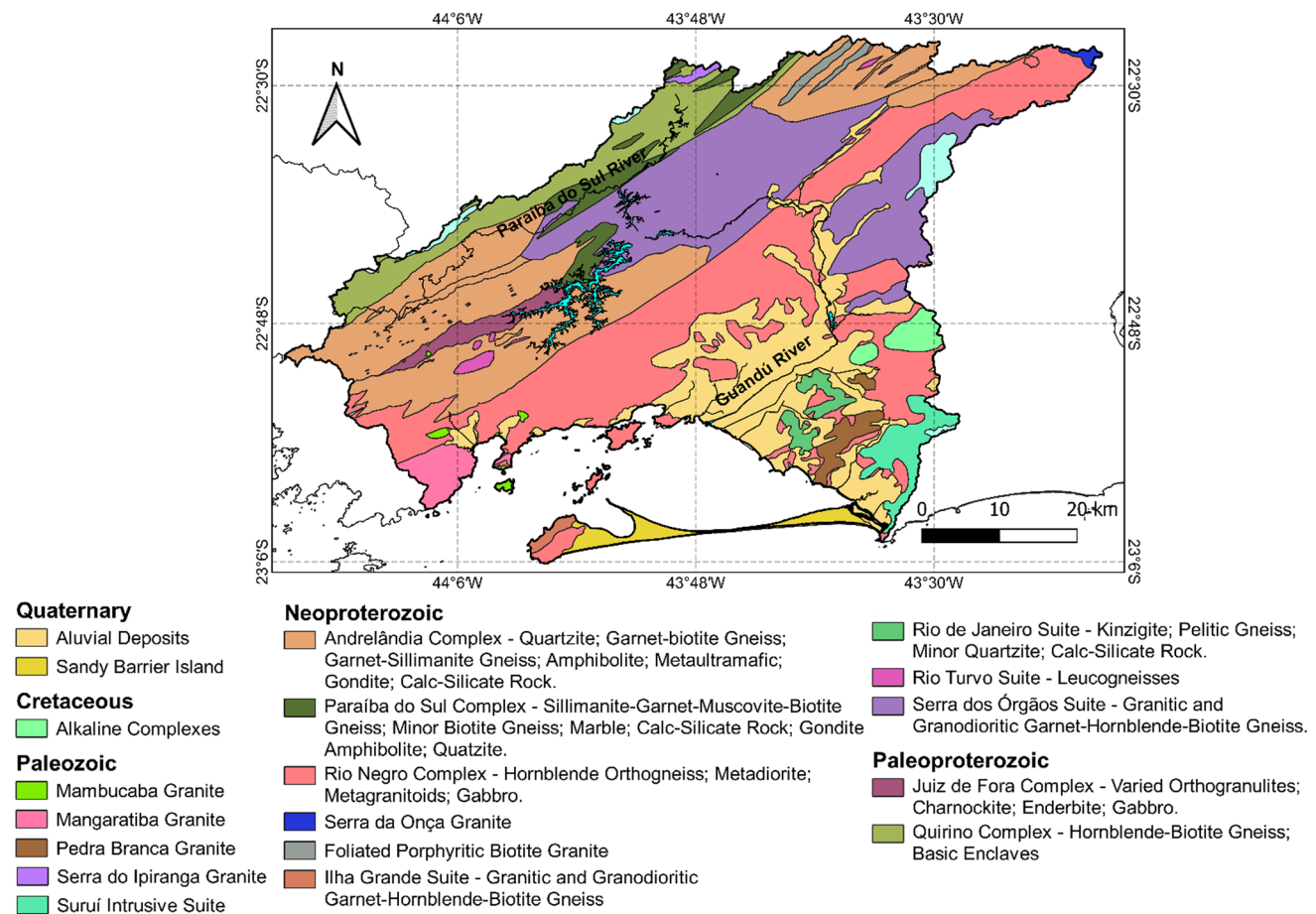


Fig. 2 Geological map of the Guandú River watershed that flows into Sepetiba Bay. Slightly simplified geology, according to Heilbron et al. (2016). The watershed boundaries were taken from Tubbs Filho et al. (2012)

collected at Guaíba Island (23° 0' 0" S, 44° 1' 9" W) indicate that the average tidal range is 0.74 m. The mean neap tidal range is ~0.3 m, while during spring tides, it is ~1.1 m, reaching up to 1.41 cm (Kjerfve et al. 2021). Therefore, according to the Davies (1964) classification, Sepetiba Bay is a micro-tidal environment.

The humid tropical climate, with high rainfall rates, influences the sculpture of the relief forms and causes profound alteration on the rocks, favoring the formation of weathering layers of varied thicknesses (SEMADS 2001) and the formation of sediments. Tectonic structures control the drainage pattern (Khan et al. 2015; Nascimento et al. 2019). Thirty-five water courses flow into Sepetiba Bay. From these, the Guandú River is the primary source of freshwater to Sepetiba Bay. Its waters reach the bay mainly through the São Francisco channel, with an annual discharge of $\sim 6.5 \times 10^9$ m³, representing 86% of the freshwater runoff (Molisani et al. 2004).

Rivers originating from the escarpment of the Serra do Mar facing the Atlantic Ocean and draining into the

Sepetiba coastal plain (SEMADS 2001) cross the lithological formations of the region, favoring the deposition of sediments in the tidal flats and mangroves along the northeast and southeast edges of the bay (Montezuma 2012; Roncarati and Carelli 2012). The estimated fluvial sediment discharge to the bay is approximately 1,150,000 t/year (SEMADS 2001).

Thus, while the northern and northeastern sectors of Sepetiba Bay are regions of high levels of sedimentation due to the fluvial input, the central sector near the Marambaia Barrier Island seems to be an erosion zone (Pereira and Santos 2012; Dadalto et al. 2021). Carvalho et al. (2020) applied a grain size trend model to surface sediments collected along the barrier up to ~2 m depth. They identified a region of divergence of sediment transport toward Ponta da Pombeba (westward) and eastward. As described by Pereira (1998), the areas of erosion and deposition observed within Sepetiba Bay are a consequence not only of the location of the sediment sources but also of the bay's internal circulation.

Materials and methods

Sampling

This work is based on the study of the sediment core SP9 (128 cm long) collected ~950 m away from the margin of Marambaia Barrier Island (Fig. 1). Core SP9 was collected in 2015 by divers (local depth ~2.3 m) using a percussion drilling method, at coordinates 23° 2' 21.00" S and 43° 51' 28.57" W. After collection, the core was preserved frozen until to be processed. After a Geotek geophysical probe was analyzed at the Marine Geology Laboratory of Universidade Federal Fluminense (LAGEMAR/UFF), X-ray images were obtained at the Nuclear Instrumentation Laboratory (COPPE/UFRJ) of Universidade Federal do Rio de Janeiro. It was opened and visually described, photographed, and sampled every 2 cm. Sediment samples were submitted to textural, mineralogical, and geochemical analyses.

Geophysical data

The following geophysical data were acquired at the Laboratory of Sedimentology (LAGEMAR/UFF): resistivity, magnetic susceptibility, and P-wave velocity. The electrical resistivity was measured with a sensor developed by the British Geological Survey and the University of Leicester. This sensor induces a high-frequency magnetic field from a transmission coil, which generates electric currents with intensities inversely proportional to the electrical resistivity. The induced electric current regenerates magnetic fields measured by a receiver coil. The technique compares the readings generated from the measuring coils to those generated from an identical set of coils operating in the air (Geotek 2016b). The recommended calibration is performed using tubes filled with water of known salinities (and, therefore, known resistivities). Magnetic susceptibility (MS) was measured with a Multi-Sensor Core Logger (MS2C; Bartington Instruments). It operates from an oscillator circuit that produces an alternating (0.565 kHz) non-saturating magnetic field of low intensity (about 80 A/m RMS). Approaching materials around the sensor cause a change in the frequency of the oscillator, provided this material has a magnetic susceptibility. The MS values are positive if the magnetic field is strengthened by paramagnetic, ferromagnetic, ferrimagnetic, or antiferromagnetic material. If, on the other hand, the magnetic field is weakened by the influence of the presence of diamagnetic material, negative MS values will be recorded (Geotek 2016a, b).

The P-wave velocity was measured with the Geotek geophysical probe. P-wave propagation occurs through

the vibration of particles in the direction of their propagation. For homogeneous and isotropic media, the P-wave propagation velocity (V_p) is expressed by the equation (Schön 1996):

$$V_p = \sqrt{((K + 1/4\mu)/\rho)},$$

where K is the compression modulus, μ is the stiffness modulus, and ρ is the density.

The P-wave velocities analyzed in core SP9 were compared with those recorded in cores SP12 (Lat. -23.036207; Long. -43.702817), SP13 (Lat. -23.052172; Long. -43.770516) and SP14 (Lat. -23.046289; Long. -43.837174). The mentioned cores were collected in Sepetiba Bay near the core SP9 and Marambaia Barrier Island in the same period (2015) and with the same sampling procedure.

Sedimentological data

Sieving methods carried out sediment grain size analysis. Fine sediments were separated from coarser sediments by wet sieving through a 63 μm sieve of a known amount of dry sediment sample ($\cong 30$ g). The > 63 and < 63 μm fractions were oven-dried and weighed. The sand and gravel fractions (> 63 μm) were separated through a series of sieves (2000, 1000, 500, 250, and 125 μm). The fine fraction < 63 μm was analyzed on a Malvern Mastersizer 2000 Size (model hydro 2000MU), and the percentage of each particle size fraction was determined.

Sediment total organic carbon (TOC) and $\delta^{13}\text{C}$ contents of the organic matter were analyzed in decarbonated samples (with 50% hydrochloric acid) with the Costech Instruments Elemental Combustion System coupled to a Delta V Thermo Scientific Advantage Isotope Ratio Mass Spectrometer (EA-IRMS), at the Laboratory of Marine Organic Chemistry (LabQOM, University of São Paulo, Brazil). The total nitrogen (N) and $\delta^{15}\text{N}$ values of the organic matter in the samples (total sediment) were also determined with the EA-IRMS at LabQOM. The following standards were used to determine stable isotopes: for $\delta^{13}\text{C}$, the Vienna Pee Dee fossil (V-PDB) and for $\delta^{15}\text{N}$, atmospheric nitrogen (Groot 2009). The USGS-40 (United States Geological Survey) and the IAEA-600 (International Atomic Energy Agency) were certified reference materials used in this analysis. Mineralogical data were obtained by X-ray diffraction of the fine fraction of the sediments at the University of Aveiro, Portugal, based on the methodology described by Martins et al. (2007).

The elemental concentrations in core SP9 were analyzed by Inductively Coupled Plasma Mass Spectrometry (ICP-MS) after digestion with 4 acids ("Near Total Digestion":

HNO₃–HClO₄–HF–HCl) at Activation Laboratories LTD., Ontario, Canada. The molecular concentrations of some oxides (Al₂O₃, Fe₂O₃, MgO, CaO, Na₂O, K₂O, TiO₂, P₂O₅, MnO, Cr₂O₃) also were estimated. About 5 g of (total) dry sediment from each sample was prepared for geochemical analyses. The samples were macerated and disaggregated in an agate mortar, sieved through a 63 μm mesh, and then geochemically analyzed at Activation Laboratories LTD., Ontario, Canada.

Geochemical data analysis

Numerous studies revealed that siliciclastic sedimentary rocks' chemical composition is linked to their source materials (Akkoca et al. 2019). Therefore, ratios between trace elements and discrimination functions are used to identify sediments' provenance (Roser and Korsch 1986; Armstrong-Altrin et al. 2013; Akkoca et al. 2019). Some trace elements that reach higher concentrations in mafic (Sc, Cr, and Co) or felsic (La, Th and REE) rocks are considered essential tools to determine the composition of the source rocks (Armstrong-Altrin et al. 2004; Zaid and Gahtani 2015). On the other hand, most elements, especially Na, K, Ca, and Mg, are partially leached out during weathering of source rocks. However, Al, Ti, and Zr can be considered immobile due to the low solubility of the oxides and hydroxides of these elements in aqueous solutions at low temperatures (Stumm and Morgan 1981; Ayers and Watson 1993; Ziemiak et al. 1993). Therefore, several ratios were used in this work to identify both the source area of the sediments and their degree of weathering and paleoclimate and paleosalinity changes.

The index of compositional variability (ICV) and the chemical index of alteration (CIA) have been used to examine geochemical variability due to hydraulic sorting and the degree of weathering of the source rock (Cullers 2000; Armstrong-Altrin 2015; Armstrong-Altrin et al. 2015a, b; Ndjigui et al. 2018).

The index of chemical variability (ICV) was calculated using the formula (Cox et al. 1995): $(\text{Fe}_2\text{O}_3 + \text{K}_2\text{O} + \text{Na}_2\text{O}^* + \text{CaO}^* + \text{MgO} + \text{MnO} + \text{TiO}_2) / \text{Al}_2\text{O}_3$. This index evaluates the ratio of alumina, which is more abundant in clay minerals, to other cations that are more abundant in non-clay minerals. This index does not use the silica (SiO₂) value to reduce quartz dilution's influence. The chemical index of alteration (CIA) can be determined by the formula (McLennan et al. 1993): $[\text{Al}_2\text{O}_3 / (\text{Al}_2\text{O}_3 + \text{CaO}^* + \text{Na}_2\text{O} + \text{K}_2\text{O})] \times 100$. This index is based on the fact that feldspars are among the most abundant minerals in the Earth's crust (Wedepohl 1969) and among the groups most easily weathered (Goldich 1938). When feldspars degrade, they form clay minerals (phyllosilicates with Al in their crystal-chemical composition). Calcium, sodium, and potassium are generally removed from

the feldspars during intense weathering processes, typically increasing the concentrations of Al (related to the abundance of phyllosilicates) in the degraded materials (Nesbitt and Young 1982). Thus, CIA is generally used to determine weathering conditions in the source area of sedimentary rocks.

Besides lithogenic sources, there are also anthropogenic sources in the sediments of Sepetiba Bay, such as potentially toxic chemical elements (PTEs). The importance of the contribution of these sources was evaluated using several indicators, such as enrichment factor, Geoaccumulation Index (I_{geo}), and concentration factor.

The enrichment factor (EF) of the chemical elements was determined using the Eq. (1) proposed by Buat-Menard and Chesselet (1979):

$$EF = \frac{\left(\frac{C_x}{C_n}\right)_{\text{Environment}}}{\left(\frac{C_x}{C_n}\right)_{\text{Baseline}}}, \quad (1)$$

where C_x is the concentration of the element under analysis, and C_n is the concentration of the normalizing element. Sc was used as the normalizing element because it is related to fine-grained sediments and, thus, reduces the influence of grain size on the concentration of the chemical elements. The baseline values from Pinto et al. (2019) were used.

The accumulation index (I_{geo}) was determined according to the following formula (2) (Müller 1986):

$$I_{\text{geo}} = \left[\frac{C_n}{B_n \times 1.5} \right], \quad (2)$$

where C_n is the concentration of metal n in the sample, and B_n is its baseline concentration.

The ecological risk index (RI) of each potentially toxic element (PTEs: As, Cd, Cu, Ni, Pb, Zn) identified in the study area was estimated by the Eq. (3) (Håkanson 1980):

$$RI = T_{\text{rf}} \times CF, \quad (3)$$

where T_{rf} is the toxic response factor for each analyzed metal. The following values of T_{rf} were considered: Zn = 1; Cu = Ni = Pb = 5; As = 10 and; Cd = 30 (Håkanson 1980; Swarnalatha et al. 2013; Yuan et al. 2014; Li et al. 2018; Rodríguez-Espinosa et al. 2018; Kükrer et al. 2020; Zheng et al. 2020). CF is the concentration factor that estimates the enrichment of an element (C_n) relative to its baseline concentration (B_n) in sediments (Eq 4) (Håkanson 1980):

$$CF = C_n / B_n. \quad (4)$$

The sum of the individual potential risks (RI) was used as the index of potential ecological risk (Eq 5) (PERI; Swarnalatha et al. 2013):

$$\text{PERI} = \Sigma \text{RI} = \Sigma (T_{\text{rf}} \times \text{CF}). \quad (5)$$

The criteria used to rank the referred geochemical indices were those suggested by Sutherland (2000) for EF; Müller (1986) for Igeo, Protano et al. (2014) for RI, and Håkanson (1980) and Swarnalatha et al. (2013) for PERI (Table S1).

The Pollution Load Index (PLI) also was estimated with the equation of Tomlinson et al. (1980) as (Eq 6):

$$\text{PLI} = \sqrt[n]{\text{CF}_1 \cdot \text{CF}_2 \cdot \text{CF}_3 \cdot \dots \dots \dots \cdot \text{CF}_n}, \quad (6)$$

where CF is the contamination factor for each analyzed metal: C_s/C_b ; metal concentration in the stratum (s)/respective baseline concentration (b). According to Tomlinson et al. (1980) PLI values > 1 suggests degradation of the environmental conditions.

Statistical analysis of the results

Selected data were log ($X + 1$) transformed and submitted to statistical analysis. To analyze the possible relationship between the variables along the core SP9, Spearman correlations for non-parametric data were determined. Correlations with $p < 0.05$ were considered significant.

The first principal component analyses (PCA) score factors were plotted as a function of depth, aiming to integrate the information extracted from the most relevant variables. Only variables with significant correlation ($p > 0.50$) with one PCA factor were used. Statistical analysis was performed in the software Statistica 13.

Core dating

The ages along core SP9 were evaluated by applying the ^{210}Pb and ^{137}Cs dating methods, which have been widely used to determine the ages of sedimentary layers deposited over a period < 150 years (Appleby and Oldfield 1978; Kamman and Engstrom 2002; Begy et al. 2011; Sabaris and Bonotto 2011; Gharibreza et al. 2013), i.e., it covers the start of the industrial age at the end of the nineteenth century. The ^{210}Pb has a half-life of 22.3 years and is a member of the ^{238}U series, with a wide distribution throughout the Earth. During radioactive decay, it releases ^{222}Rn gas (daughter of ^{226}Ra) from the soil and sediments into the atmosphere. The short ^{222}Rn (3.82 days) decays to ^{210}Pb , which returns to the land or aquatic/marine surface within weeks as solid precipitation. The ^{210}Pb activity can be supported, produced in situ by the natural decay of ^{226}Ra , and unsupported, sourced from atmospheric fallout.

The unsupported part can be used to determine the age of the sediment layer. As the sediment is buried under more recent layers, the unsupported activity declines, following the law of natural decay. Therefore, the unsupported ^{210}Pb acts like a natural clock, recording when it has been deposited in soils and sediments. Thus, the current activity C_{excess} (measured) can be inscribed as a function of the age and the initial activity when the sediment was buried $C_{\text{excess}}(0)$ (Eq. (7); Appleby 2008).

$$C_{\text{excess}}(t) = C_{\text{excess}}(0) \times e^{-\lambda t}. \quad (7)$$

Estimating this isotope's initial activity allows the sediment's age to be accurately determined. Commonly, two models have been used to address the geochronology based on this method: the constant rate of supply (CRS) model, which considers the occurrence of a constant flux of unsupported ^{210}Pb to the sediment and allows estimation of a variable sediment rate (Appleby and Oldfield 1978; Appleby 2001). The CRS model's initial concentration varies inversely with the sedimentation rate. In the CIC model, which is based on a constant initial concentration, the ^{210}Pb amount varies directly with the sedimentation rate (Appleby 2001). The CIC model considers that the sediment is deposited with a constant flux, so the sedimentation rate is also constant (Shukla and Joshi 1989; Godoy et al. 1998). If sedimentation rates remained relatively constant, the CRS and CIC models would provide the same result.

The Pb model was validated using independent ages determined from records of the artificial ^{137}Cs fallout radionuclides ($T_{1/2}$ of 30.2 years) (Pennington et al. 1973; Appleby 2008). The ^{137}Cs is an anthropogenic radionuclide released into the atmosphere in the early 1950s following the first nuclear weapon testing (Figueira et al. 2007). In the Southern Hemisphere, to be able to determine the sedimentation rate in sediment cores, it is necessary to identify the peak of the highest intensity of ^{137}Cs , corresponding to the year 1963, related to the highest intensity of nuclear tests (Figueira et al. 2007).

Samples collected every 4 cm along the core SP9 were submitted to ^{210}Pb and ^{137}Cs analyses. About 15 g of the fine fraction of the sediment (> 63 μm) dried and macerated were prepared for these analyses. The analysis was conducted at the Oceanographic Institute of the University of São Paulo (IO-USP) in the Marine Inorganic Chemistry Laboratory (LAQIMAR). The Constant Sedimentation Model (CFCS—Constant Flux: Constant Sedimentation; Koide et al. 1973; Brugam 1978; Appleby and Oldfield 1978, 1983), the constant initial concentration of unsupported ^{210}Pb (CIC; Robbins and Edgington 1975; Matsu-moto 1975), and the Variable Sedimentation Model (CRS) based on unsupported/ excess ^{210}Pb , following the guidelines of Figueira et al. (2007) and Ferreira et al. (2015), were used

to estimate the age model and the sedimentation rate of core SP9 (Appendix 1).

Some geochemical results from core SP9 were compared with those of other cores collected in the Sepetiba Bay to broaden the data interpretation: SP3 (Castelo et al. 2021a, b), SP5 (Silva et al. 2022a, b) and SP6 (Alves Martins et al. 2019). From core SP6, only the first top 40 cm of the sedimentary column that records the period since 1955, according to the model data based on ^{210}Pb and ^{137}Cs methodologies, are used in this work (Appendix 2). The age models of these cores are included in Appendix 1. The ages used in this work are from calendar years or Anno Domini (AD).

Results

Core characteristics and age model

Core SP9 consists mainly of gray to dark gray fine sediments (Fig. 3A; Appendix 3). X-ray imaging showed faint sedimentary structures (low-angle parallel laminations) in the upper 20 cm and changes at 42 and 76–80 cm; slightly higher values of magnetic susceptibility occur between this depth and the core base (Fig. 3A). Magnetic susceptibility (2.3 and 16.7 SI) reaches higher values at the lower part of the core, decreasing significantly at the top (Fig. 3A). The resistivity (0.4–6.4 Ωm) is constant along the core, except around 60 cm and close to the top (Fig. 3A). P-wave velocity shows relatively high values (maximum of 1561 m s^{-1}) in the lower and upper sections of the core. However, it decreases between 100 and 56 cm and, most significantly, around 60 cm (where it reaches a minimum value of 255 m s^{-1}). A similar reduction in P-wave velocity was also observed in cores SP12, SP13, and SP14 (Fig. 3B).

The age of sediment layers, obtained by ^{137}Cs and ^{210}Pb methods through the CIC and the CRS models for core SP9, is shown in Fig. 4 (and Appendix 1). The SP9 core records the peak of ^{137}Cs at the 46 cm level, equivalent to 1963, corresponding to the maximum fallout from the atmospheric nuclear weapons test (Appleby et al. 1991). By the CRS model, the year 1965 was estimated for this level. A good agreement was observed between the ages of the sediment layers estimated by both ^{210}Pb models and ^{137}Cs (Appendix 1). The estimated age models allow us to verify that the age of the core base is older than 1866 and is beyond the limit of 7 half-lives of ^{210}Pb . Therefore, the sedimentary records up to about 1855 were considered in this work.

According to the CRS model, the mean sedimentation rate varied between 1.32 ± 0.09 and 0.08 ± 0.01 cm yr^{-1} , and the average mass accumulation rate was about 0.14 ± 0.01 $\text{g cm}^2 \text{yr}^{-1}$ (Appendix 1). The mean sedimentation rate was highest at the upper part of the core (between 1970 and 2015) and reduced significantly in sediment layers deposited before

1970, reducing after that to values $< 0.14 \pm 0.02$ cm yr^{-1} (Appendix 1).

Particle size characteristics

According to the classification of Shepard (1954), core SP9 consists of very poorly sorted clayey silt at the lower part and silty sediments at the upper section. The most abundant fine fractions are fine silt (~49%), clay (~16.2%), and medium silt (~12.5%). The fine fraction ($< 63 \mu\text{m}$) is predominant (48.8–96.2%; mean $88.9 \pm 10.7\%$), mainly in the lower section of the core. The percentage of the sand fraction increases (3.8–51.2%; mean: $11.1 \pm 10.7\%$) at the top of the core, between 30 and 0 cm, due to increasing contents of very fine, medium and coarse sand fractions. The percentage of fine silt and clay is reduced in the upper core section (Fig. 3A). The remaining fine fractions are a little variable throughout the core.

Mineralogical composition

The main minerals identified in the fine fraction of core SP9 are, in descending order, phyllosilicates (32.0–72.9%; mean 52.2%), quartz (20.6–52.8%; mean 36.2%), and feldspars (2.1–32.6%; mean 7.5%). Some minerals with an abundance below 10% were identified only in a few layers, such as anatase, anhydrite, bassanite, calcite, gypsum, ilmenite, magnetite/maghemite, pyrite, rhodochrosite, siderite, zeolites. Anatase, pyrite, siderite, and anhydrite reach maximum values between 5 and 7%, while the remaining minerals exhibit relative abundances $< 5\%$ (Appendix 1).

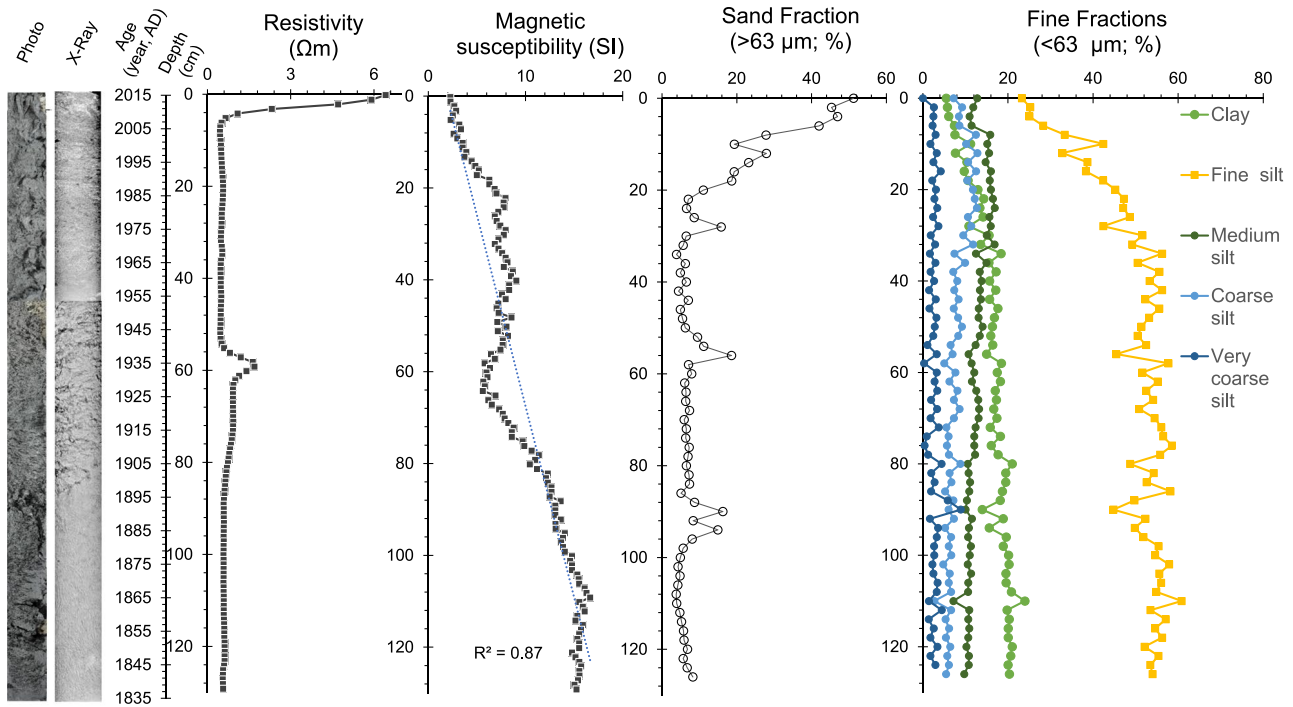
The abundance of the main minerals (phyllosilicates, quartz, and feldspars) oscillated around their averages without a clear distribution pattern throughout the core (Fig. S1). Calcite, although not abundant ($< 2.43\%$; average 1.0%), exhibits a slight increase in the upper section of the core (Fig. S1).

TOC and N contents, and $\delta^{13}\text{C}$ and $\delta^{15}\text{N}$ values

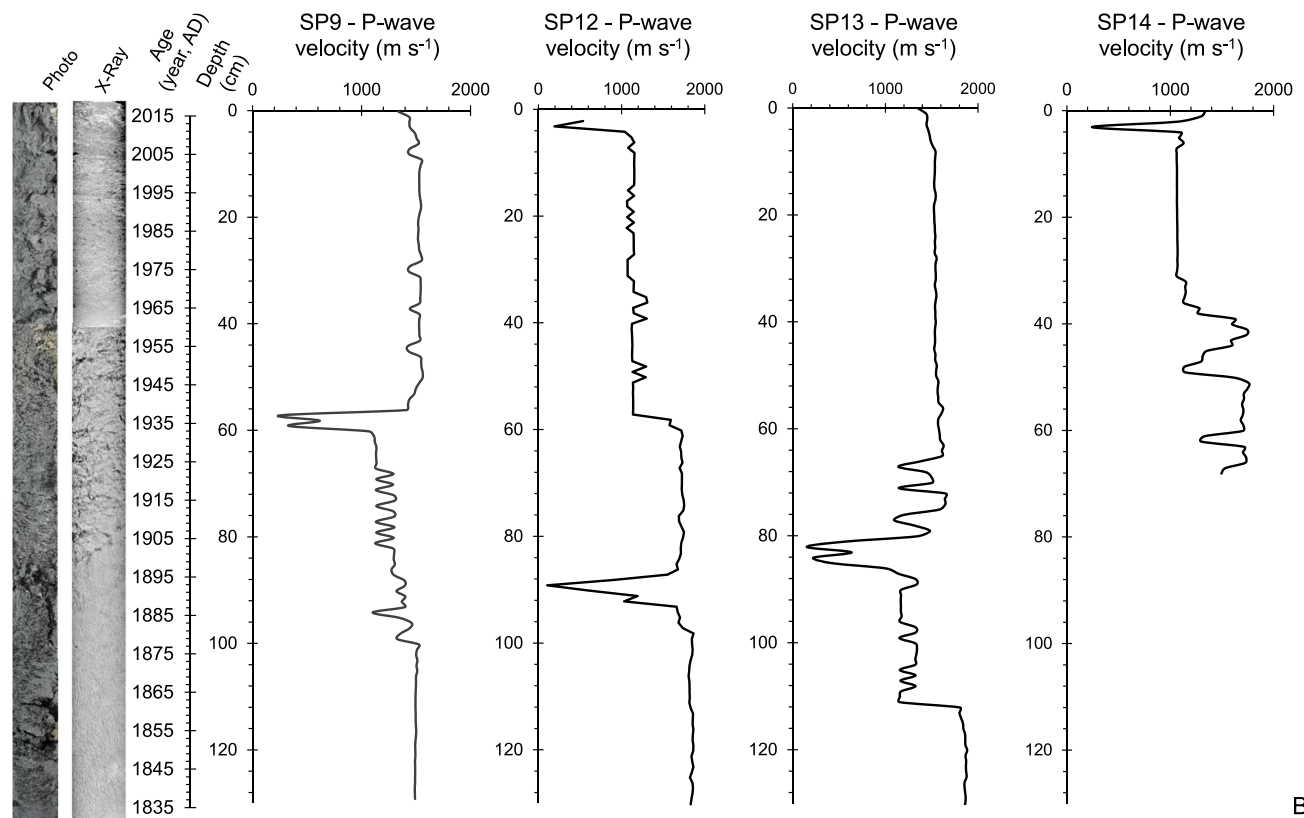
TOC contents vary significantly along the core SP9 (0.7–3.38%; mean $1.3 \pm 0.4\%$). Excluding the TOC peak of 3.38% recorded at the 42 cm level (≈ 1968), the regression line and the respective R^2 value (0.82) for the remaining levels indicate a clear progressive upward trend in the supply of organic carbon contents (Fig. 5; Appendix 3).

Nitrogen contents (0.09–0.24%; mean $0.16 \pm 0.03\%$) followed a similar pattern; the lowest N values were recorded in the lower part of the core. Like TOC, N contents increased upward (Fig. 5; Appendix 3).

The $\delta^{13}\text{C}$ values (-25.5 to -20.2‰ ; mean: $-21.1 \pm 0.9\text{‰}$) show a few peaks relative to the mean, with the most significant deviation (-25.5‰) being observed



A



B

Fig. 3 **A** Depth plots of resistivity, magnetic susceptibility (SM), the sand fraction (> 63 μm; %), and fine fractions (> 63 μm) along the core SP9. **B** P-wave velocity (m s⁻¹) along the core SP9 is compared

with that of core SP12, SP13, and SP14. These cores were collected near the core SP9 (Fig. 1). A photo, an X-ray imaging, and an age scale are also represented in **A** and **B**

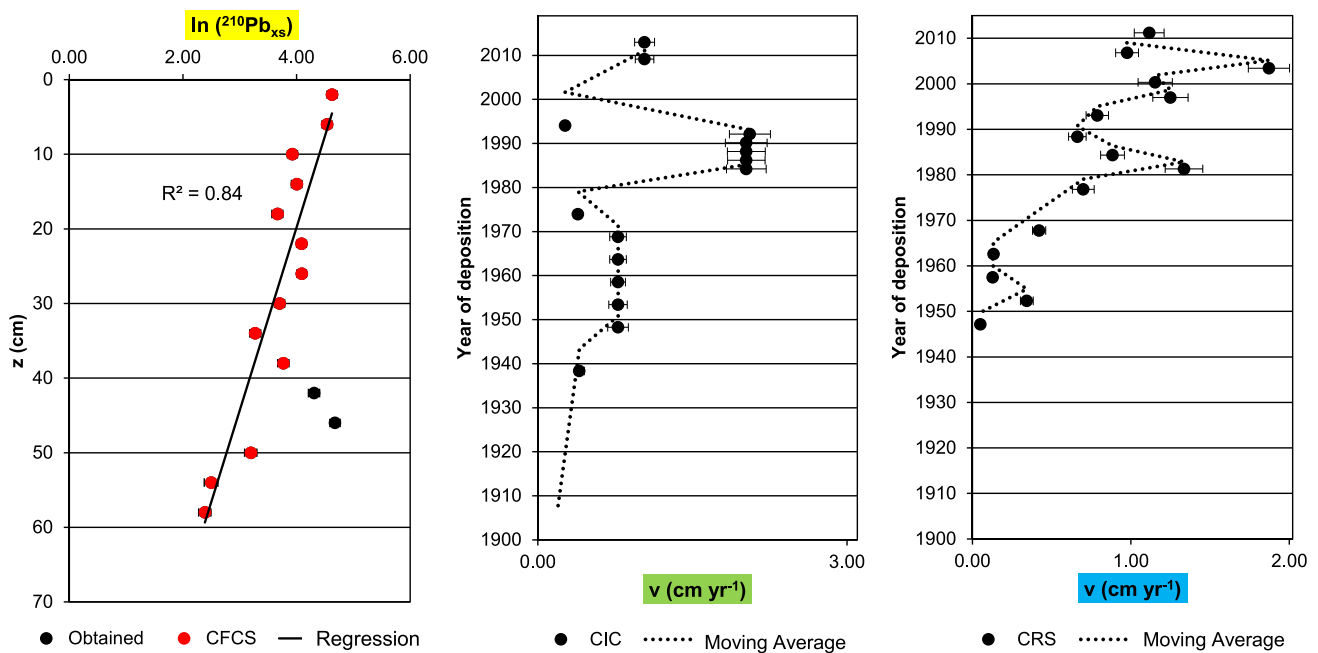


Fig. 4 Age models of core SP9 based on ^{210}Pb . Legend marked: yellow—constant sedimentation model (CFCS); green—constant sedimentation model (CFCS); blue—variable sedimentation model (CRS)

recorded at ≈ 1968 (42 cm level; Fig. 5; Appendix 3). The $\delta^{15}\text{N}$ values ($8.4\text{--}11.7\text{‰}$; mean $10.4 \pm 0.9\text{‰}$) are slightly higher between the core base and ≈ 1960 (50 cm level); they decreased significantly since 1957 (50 cm), but have a peak in ≈ 1997 and 2007 (22–6 cm; Fig. 5; Appendix 3). The carbonate concentration is less than 15%, but shows two peaks, the first round in 1990 and the second since 1995 (in the upper core section; Fig. 5; Appendix 3).

Elemental and oxide concentrations

The ranges of elemental and oxide statistics concentrations (maximum, minimum, mean, and standard deviation values) along core SP9 are presented in Appendix 3. The distribution of elemental concentrations shows upward increasing trends for: Zn ($81\text{--}935\text{ mg kg}^{-1}$; mean: $328 \pm 305\text{ mg kg}^{-1}$), Cd ($< 5.9\text{ mg kg}^{-1}$), Mn ($362\text{--}1370\text{ mg kg}^{-1}$, mean $663 \pm 248\text{ mg kg}^{-1}$), P ($0.05\text{--}0.08\%$; $0.06 \pm 0.01\%$), Ni ($22.1\text{--}30.0\text{ mg kg}^{-1}$; mean: $24.7 \pm 1.7\text{ mg kg}^{-1}$), Pb ($24.0\text{--}38.0\text{ mg kg}^{-1}$; mean: $30.1 \pm 4.9\text{ mg kg}^{-1}$), Cu ($11.0\text{--}32.6\text{ mg kg}^{-1}$; mean: $16.1 \pm 4.8\text{ mg kg}^{-1}$) and As ($3.0\text{--}15.0\text{ mg kg}^{-1}$; mean: $6.6 \pm 3.0\text{ mg kg}^{-1}$). Significant increases in Zn, Cd, and Pb concentrations have been observed since ≈ 1955 . There has been a gradual upward trend in Mn, P, Ni, As, Cu, Cr, and Fe concentrations since 1915, but significant increases in these elements have been observed since 1975 (Fig. 5).

Calcium, Mg, Ti, and Zr contents of core SP9 were compared with those obtained in cores SP3 (Castelo et al. 2021a,

b), SP5 (Silva et al. 2022a, b), and SP6 (Alves Martins et al. 2019). The results presented in Fig. 6 show that Ca contents ($0.3\text{--}1.2\%$; mean $0.5 \pm 0.3\%$) are low in cores SP9, SP3, SP5, and SP6; however, they are generally higher in core SP9 than in cores SP3, SP5, and SP6, and tend to increase at the top (upper 20 cm), since 1990.

Magnesium concentrations are, in general, higher in core SP9 than in cores SP3, SP5, and SP6, being only surpassed in core SP5 between ≈ 1945 and 1963 and around ≈ 1963 and in core SP3 between ≈ 1992 and 1996 (Fig. 6). Titanium contents ($0.2\text{--}0.5\%$, mean $0.4 \pm 0.2\%$) in core SP9 are similar to that recorded in the other cores except between ≈ 1855 and 1924 in core SP5 (Fig. 6). The distribution pattern of Zr is similar to that of Ti (Fig. 6). Zr concentrations are generally higher in core SP9 than in the other cores, except in core SP5 that reaches highest contents between ≈ 1855 and 1924, as Ti (Fig. 6). However, since 1935, several rises of Zr concentrations were observed.

The values of the ratios La/Sc, La/Cr, Ti/Ca, Fe/Ca Th/Cr, Th/Sc, Zr/Sc, and Zr/Cr are not variable in the SP9 core (Fig. 6). The most significant increases La/Sc, La/Cr, Th/Cr, Th/Sc, Zr/Sc, and Zr/Cr ratios were recorded between ≈ 1855 and 1920 in core SP5 and between ≈ 1915 and 1975 in the core SP3 (Fig. 6).

The values of $\text{Al}_2\text{O}_3/\text{TiO}_2$ and Rb/K are, in general, higher in core SP9, than in the other cores SP3, SP5, and SP6 (Fig. 7). In contrast, the values of $\text{V}/(\text{V} + \text{Ni})$ and Rb/Sr ratios are lower in core SP9 than in the other cores (Fig. 7). The distribution pattern of the Rb/Sr and Rb/K values is

opposite (Fig. 7). All these ratios show a pattern with cyclical increases and decreases along the core SP9 (Fig. 7). The changes of $\text{Al}_2\text{O}_3/\text{TiO}_2$, $\text{V}/(\text{V} + \text{Ni})$ and Rb/K are in general gradual. However, cyclic changes in Rb/Sr values were also observed in the core SP5, where the values of this variable reached relatively high values.

Enrichment factors (EF) and pollution load index (PLI)

The estimated EF values for most of the chemical elements in core SP9 are low ≤ 3 (Appendix 3). Higher EF values (up to 10) were reached in core SP9 for Zn and Cd. The graphs in Fig. 8 show that reduced EF-Zn and EF-Cd values were recorded before 1935 in cores SP9, SP5, and SP3. The EF-Zn and EF-Cd values increased after 1935 and more significantly since 1955. The EF-Zn and EF-Cd values in core SP9 after 1955 are similar to those recorded in core SP5. The highest EF-Cd values were observed in core SP9, while EF-Zn values were recorded in core SP5. It is worth noting that a drop in EF-Zn and EF-Cd values has been generally observed since 2005 in core SP9.

The distribution of the PLI and PERI values in core SP9 is also represented in Fig. 8 in comparison with cores SP5 and SP3. The PLI reaches higher values in core SP9 (up to 2.9) than in cores SP3 and SP5. As for the PLI, the highest PERI values (389) are also observed in core SP9. Both PLI and PERI reached higher values between 1960 and 2005, with a significant drop in 1991 and since 2005.

Statistical results

A selection of core SP9 variables was submitted to principal component analysis (PCA). In this analysis, the following variables were considered: granulometric data, such as clay ($< 2 \mu\text{m}$), fine silt ($2\text{--}8 \mu\text{m}$), total sand, and fine fraction (> 63 and $< 63 \mu\text{m}$, respectively); PTE concentrations (As, Cd, Cu, Ni, Pb, and Zn); geochemical ratios and indexes ($\text{Al}_2\text{O}_3/\text{TiO}_2$, Fe/Ca , Ti/Ca , La/Cr , Rb/Sr , Th/Sc , $\text{V}/(\text{V} + \text{Ni})$, La/Sc , Rb/K , Zr/Sc , CIA, ICV); environmental quality indicators, such as PERI, PLI and also P, Mg, Mn contents.

The Factor Loadings (Unrotated) of the two first principal components of the PCA explained 64% of the data variability (Factor 1: 47%; Factor 2: 18%). Factor 1 of PCA (Fig. 9) places the elements As, Cu, Ni, Zn, Cd, and Pb, as well as the PERI, PLI, and ICV values and sand fraction contents (II) in opposition to $\text{Al}_2\text{O}_3/\text{TiO}_2$, Fe/Ca , Ti/Ca , La/Cr , Rb/Sr , Th/Sc , and fine fraction (I). The correlations in Appendix 4 show that concentrations of PTEs (such as As, Cu, Ni, Zn, Cd, and Pb), PERI, and PLI values, have strong positive correlations with each other and sand contents, confirming the PCA results. All mentioned chemical elements (As, Cu, Ni, Zn, Cd, and Pb) have: (a) positive and significant

correlations with TiO_2/Zr and mostly with ICV, except Pb; (b) weak correlations with $\text{V}/(\text{V} + \text{Ni})$, La/Sc , Rb/K and Zr/Sc ; and (c) significant negative correlations with clay and fine silt and total fine fraction and CIA, except Cd and Pb (with negative correlations but not significant). Cd and Zn have weak negative correlations with lithogenic indicators such as $\text{Al}_2\text{O}_3/\text{TiO}_2$, Fe/Ca , Ti/Ca , La/Cr , Rb/Sr , and Th/Sc . Significant negative correlations are also observed between As and $\text{Al}_2\text{O}_3/\text{TiO}_2$, Fe/Ca , La/Cr , Rb/Sr , TiO_2/Zr , and CIA; Cu and Fe/Ca ; Ni and Fe/Ca , La/Cr , Rb/Sr ; and Pb and Th/Sc . It is further observed that Factor 2 is positively associated with Zr/Sc and Th/Sc , as well as with ICV, $\text{V}/(\text{V} + \text{Ni})$, La/Sc , and Rb/K .

The biplots of the two first principal components of the PCA for a similar set of variables have also been plotted in Fig. 9 for cores SP5 and SP3. In both cases, the first two factors explain most of the data variability: (a) in core SP3, they explain 77% of the data variability (Factor 1: 64%; Factor 2: 13%), and (b) in core SP5 (Factor 1, 54%; Factor 2, 19%) 74% (Appendix 5). In core SP3, PTEs are also negatively related to lithogenic indicators, as in core SP9 (namely with Ti/Ca , Zr/Sc , Th/Sc , La/Sc , La/Cr , $\text{Al}_2\text{O}_3/\text{TiO}_2$, and ICV), but are positively related to Rb/K , Rb/Sr and Fe values. In core SP5, the PTE enrichments are also negatively related to some lithogenic indicators (such as Th/Sc , Zr/Sc , Ti/Ca , CIA, and Rb/Sr). However, they are positively related to other variables, such as La/Th , $\text{Al}_2\text{O}_3/\text{TiO}_2$, and ICV. There is, therefore, a more remarkable similarity in the association of the PTEs with the variables studied in core SP3 and SP9.

Discussion

The granulometric and mineralogical characteristics of core SP9 reveal that the study area was under the influence of generically calm hydrodynamic activity since 1855 but with some variations. The resistivity values increase at ≈ 60 cm depth and the top of the core SP9, probably due to granulometric and compositional sediment-related hydrodynamic changes. The magnetic susceptibility values, corresponding to the degree of magnetization of a material in response to an applied magnetic field (Geotek 2016a), decrease from the bottom to the core top, indicating changes in sediment composition. Thus, we sought to understand if these features would be related to changes in sediment sources, weathering, and recycling.

Changes in the composition of the sediment

The $\text{Al}_2\text{O}_3/\text{TiO}_2$ ratio in terrigenous sediments is a helpful tool for identifying source rocks (Hayashi et al. 1997). Al is generally associated with feldspars and Ti in igneous rocks, which reach higher contents in mafic minerals (e.g.,

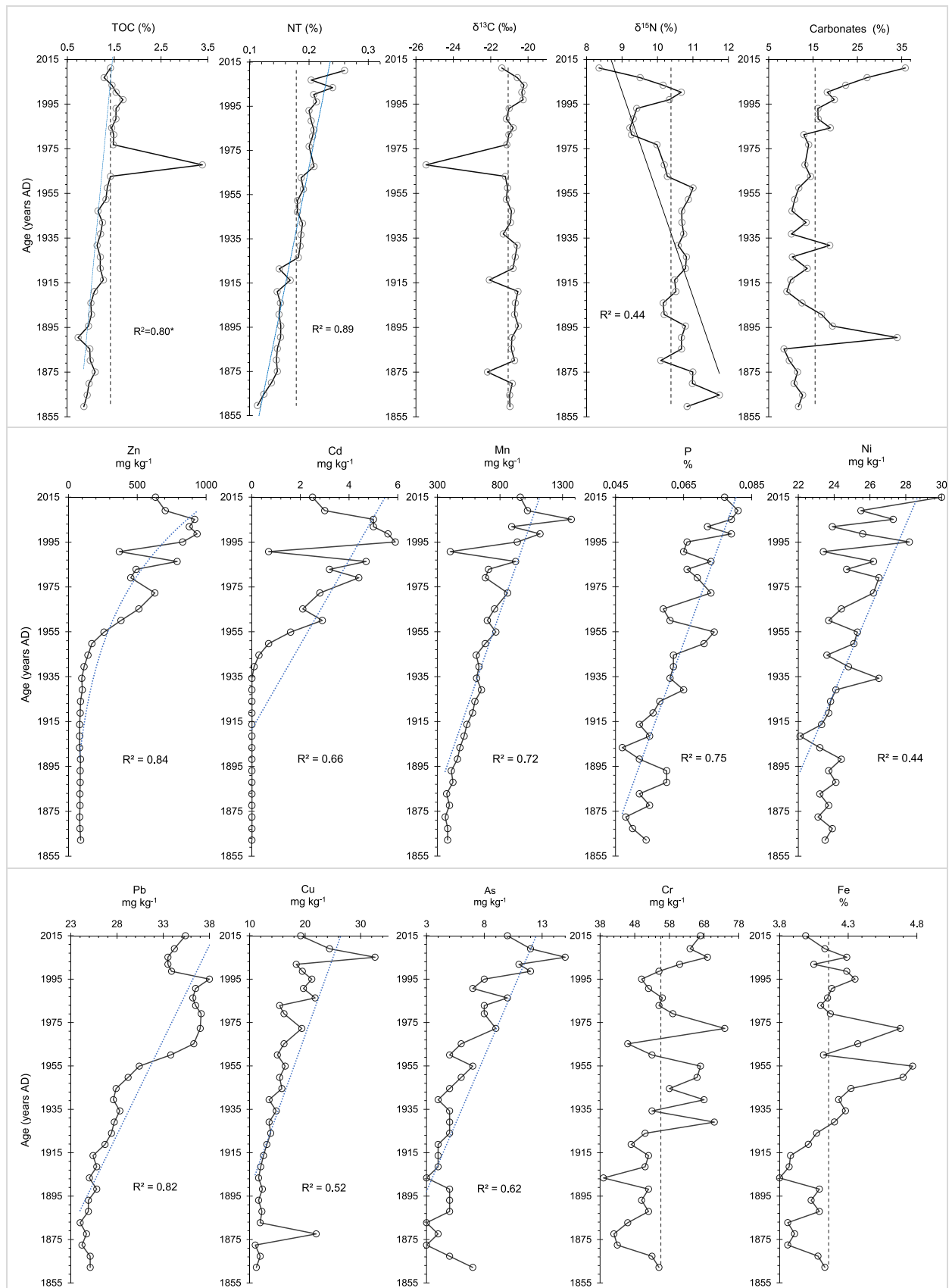


Fig. 5 Age plots of geochemical data. Circles represent values. For selected variables, their average was represented by a vertical dashed line. Regression lines and the respective R^2 were also plotted for some variables. The regression line and the respective R^2 were estimated for TOC without the high value recorded in 1968

olivine, pyroxene, hornblende, biotite, and ilmenite (Hayashi et al. 1997). The $\text{Al}_2\text{O}_3/\text{TiO}_2$ ratios in igneous rocks generally rise with increasing SiO_2 content (Hayashi et al. 1997). Thus, the values of this ratio are lowest in mafic igneous rocks ($\text{SiO}_2 = 45\text{--}52$ wt%), middle in intermediate igneous rocks ($\text{SiO}_2 = 53\text{--}66$ wt%), and highest in felsic igneous rocks ($\text{SiO}_2 = 66\text{--}76$ wt%) (Hayashi et al. 1997). Thus, the $\text{Al}_2\text{O}_3/\text{TiO}_2$ ratios increase from mafic ($\sim 3\text{--}8$) to intermediate ($\sim 8\text{--}21$) and to felsic rocks ($\sim 21\text{--}70$) (Nagarajan et al. 2017).

The depth plot of $\text{Al}_2\text{O}_3/\text{TiO}_2$ values for core SP9 (Fig. 7) indicates that it has primarily intermediate source sediments, with recurrent levels more enriched in felsic source materials. The other cores also have sediments mainly from intermediate sources. The exceptions are the base of core SP3 (deposited between ≈ 1920 and 1938), with $\text{Al}_2\text{O}_3/\text{TiO}_2$ values indicating higher felsic particles (similar to core SP9), and some levels of core SP5 (deposited between ≈ 1905 and 1915), with a more significant contribution from mafic sources. The enrichment in felsic components may result in this system from the weathering of the sediments, which results in a higher concentration of felsic minerals (e.g., quartz, which is resistant to coastal dynamics processes).

The content of Ti- and Zr-containing minerals in sediments can increase significantly during the transport and deposition of clastic sediments (Argast and Donnely 1987). Since both elements are associated with erosion-resistant minerals, Ti and Zr concentrations can provide helpful information about sediment sorting and sources.

Thus, based on the scatter plot of Zr vs TiO_2 (Fig. 10A) and in the fields suggested by Hayashi et al. (1997) it is possible to deduce that most of the sediments in the analyzed cores come from intermediate igneous rocks; they are primarily related to gneisses, abundant in the region (Tubbs Filho et al. 2012; Heilbron et al. 2016) and may have been largely supplied by the rivers flowing into Sepetiba Bay. However, it is possible to recognize that some levels of core SP9 and SP3 are mainly composed of felsic particles.

An indication of the influence of sediment transport by the rivers in the various regions of Sepetiba Bay is the variation of the average sediment accumulation rates (estimated by ^{210}Pb methods): in core SP6, it was 0.26 ± 0.04 cm yr^{-1} (Alves Martins et al. 2019), in core SP3, was 0.92 ± 0.15 cm yr^{-1} (Castelo et al. 2021a, b), in core SP5, was 0.83 ± 0.13 cm yr^{-1} (Silva et al. 2022a, b) collected in near the Guandú River mouth) and in core SP9, was 0.14 ± 0.01 cm yr^{-1} . It should be noted that according

to Molisani et al. (2004), the Guandú River contributes most of the sediment received in Sepetiba Bay. The above-average sedimentation rates denote significant sediment accumulation rate variability in different Sepetiba Bay areas. It seems to be influenced by the proximity of the rivers: higher accumulation rates near the river mouths, namely the Guandú River, and lowest averages recorded in the distal region. Variations in hydrodynamic characteristics also have a significant influence on the rate of sediment accumulation. The SP9 core located in a distal region of the bay receives a more negligible contribution of sediments introduced by the rivers into the bay. On the other hand, this area is subject to more active coastal dynamics.

Weathering and recycling of sediments

The chemical alteration index (CIA) and the compositional variability index (CVI) can show whether the sediments have undergone more or less pronounced chemical weathering processes (Cox et al. 1995; McLennan et al. 1993; Abubakar et al. 2019). CIA values: $\approx 50\%$ indicate no weathering, ranging from 60% to 80% suggest moderate weathering, and $> 80\%$ indicate the high intensity of chemical weathering (Nesbitt and Young 1982).

On the other hand, according to Goldich (1938), the higher ICV values tend to be associated with the presence of more rapidly weathered minerals, such as olivine, pyroxene, and amphibole. They tend to be lower as the abundance of phyllosilicates increases. Thus, higher ICV values (> 1) indicate immature sediments and the presence of a higher abundance of non-clayey siliciclastic minerals relative to clay minerals (Cox et al. 1995). Conversely, lower ICV values (< 1) indicate the presence of compositionally mature sediments with a high percentage of clay minerals (Long et al. 2012).

The CIA versus ICV plot presented in Fig. 10B suggests that the sediments from SP9 and the upper part of the core SP6 (analyzed in this work) are mature and have experienced moderate to intense weathering, as well as part of cores SP5 and SP3, which also have immature sediment layers. Core SP3 has moderately weathered sediments, while the other cores contain moderately to intense weathered sediment layers. Core SP9 is composed mainly of intensely weathered sediment except the top layers deposited after 2000, which contain moderately weathered sediments (Fig. S2). Core SP9 is located in an external region of Sepetiba Bay, close to the Pombeba spit and Marambaia Barrier Island, where the coastal dynamics reworks the sediments. However, the top of this core records the accumulation in this area of a significant contribution of poorly weathered particles.

Thus, comparing the data from cores SP5 and SP3, we infer that from the 1950s on, there has been a sudden change in the textural and geochemical properties of

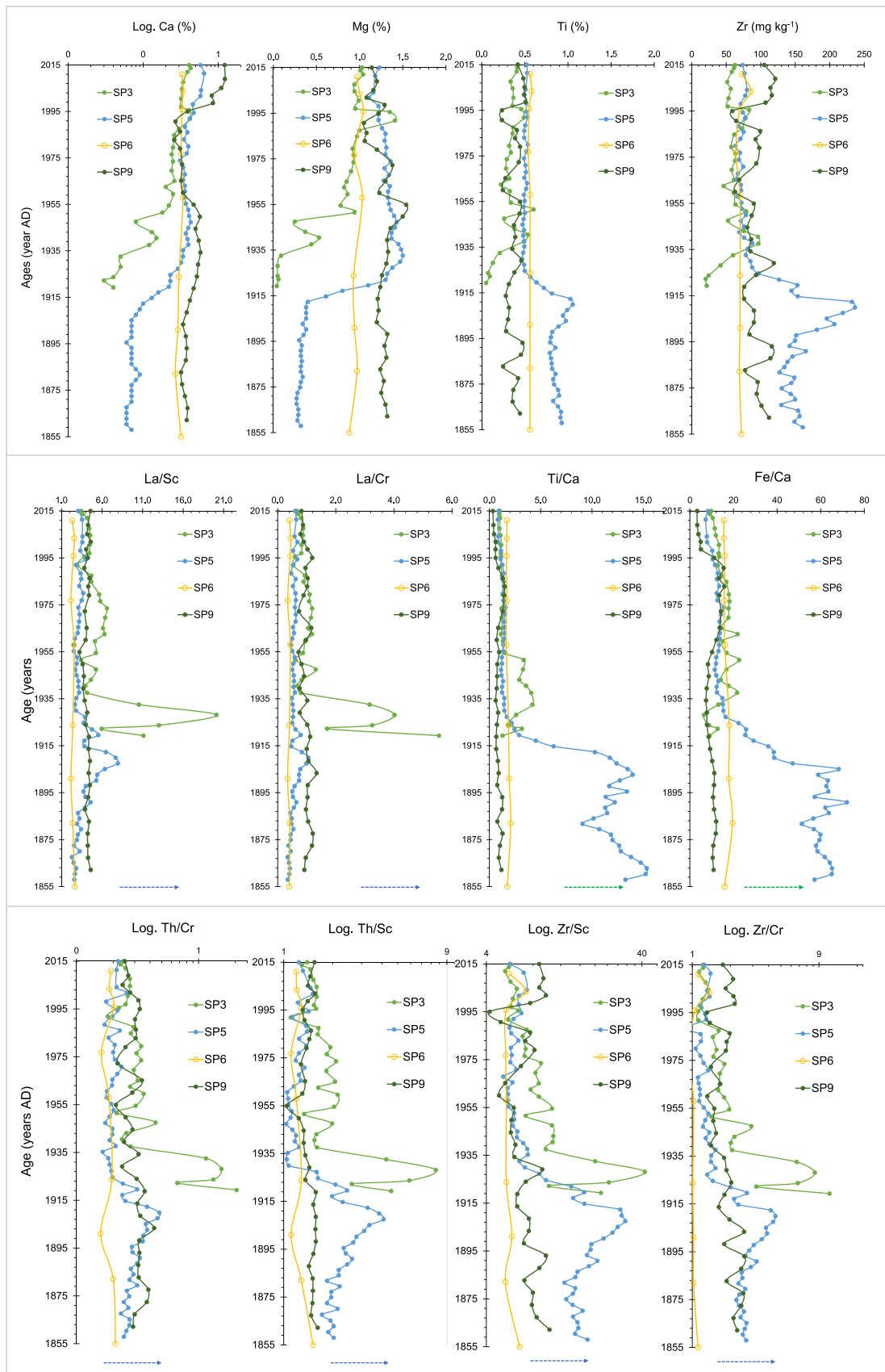


Fig. 6 Age plots of Ca (%), Mg (%), Ti (%) and Zr (mg kg^{-1}) concentrations and La/Sc, La/Cr, Ti/Ca and ratios obtained in core SP9, as well as in cores SP3 (Castelo et al. 2021a, b), SP5 (Silva et al. 2022a, b) and SP6 (Alves Martins et al. 2019). The blue arrow represents the greater accumulation of sediments from felsic sources and the green arrow indicates increased detrital sediments relative to carbonates. Age plots of Th/Cr, Th/Sc, Zr/Sc and Zr/Cr ratios were obtained in core SP9, as well as in cores SP3 (Castelo et al. 2021a, b), SP5 (Silva et al. 2022a, b) and SP6 (Alves Martins et al. 2019). The blue arrow represents the greater accumulation of sediments from felsic sources

the sediments. The transposition of the Paraíba do Sul River to the Guandú River basin since the 1950s (Macedo and Pimentel 2004) may have had a notable effect on the weathering of the sediments and on their chemistry and maturity.

In core SP9, the sediment accumulation rate was low before 1950. These data reveal that this area had, at that time, an essentially erosional character. However, since the 1950s, the sediment accumulation rate has progressively increased and was relatively high between ≈ 1980 and 2003 (up to $1.32 \pm 0.09 \text{ cm yr}^{-1}$; Appendix 1). This change may be related to the increased sediment load introduced into Sepetiba Bay and the accumulation of sediments from other sources, as explained below.

The composition of the upper part of core SP9 agrees with the characteristics of the bottom sediments currently observed in that region. The shallow region near the Marambia Barrier Island is favorable for carbonate precipitation. The bottom of that area is composed mainly of carbonate-aggregated sands. On the other hand, carbonate contents (which are essentially abiotic since carbonate shells and tests are rare) increased around 1890 and 1932 and have been progressively increasing since 1990, with a maximum peak observed in 2011–2015. These data indicate that the area of core SP9 may have been submitted to more or less pronounced evaporative processes in the past, depending on the water column height and the oceanic influence in the region. Another factor should be related to the extension and development of the Ponta da Pombeba spit (as analyzed by Dadalto et al. 2021) and the protection it provides. We can also consider the prevalence of favorable conditions for carbonate preservation.

During weathering (and, in many cases, diagenesis), an increase in Rb/Sr ratio values is observed in most rocks. It happens because Rb^+ , a relatively large alkali chemical element, is more easily retained in clay minerals than Sr^{2+} , with smaller sizes (McLennan et al. 1993). Thus, changes in the Rb/Sr ratio allow the detection of chemical weathering processes (Ohr et al. 1991). Rb occurs mainly in K-bearing minerals that are relatively stable to weathering. In the cores SP9, SP3, and SP5, Rb concentrations positively correlate with K_2O , agreeing with this assumption (Fig. S3). Sr is mainly associated with Ca-minerals that are sensitive to

weathering. Rb/Sr ratios increase with the dissolution of Ca-mineral-bearing minerals.

The Rb/Sr ratios of the analyzed cores vary between 0.69 and 1.20; they are higher than the value of the Upper Continental Crust (UCC) 0.32 (Taylor and McLennan 1985), also indicating moderate to high weathering (Fig. 7).

Organic matter supply

Nitrogen, P, and TOC values have progressively increased since 1855 (Fig. 5), as shown by the regression lines of these variables (with R^2 values between 0.75 and 0.89). These results suggest that the increase in nutrients contributed to the increased supply of organic matter to the sediment in this outer region of Sepetiba Bay despite the hydrodynamic characteristics of this area.

One of the consequences of the high accumulation of organic matter was the reduction of oxygen contents in the sediment. It was investigated using the ratio $\text{V}/(\text{V} + \text{Ni})$. This ratio was used as a paleoredox indicator of the environment since V tends to precipitate under reducing conditions and dissolve in oxidizing environments. Ni is more stable than V in both situations (Hatch and Leventhal 1992; Arthur and Sageman 1994). Therefore, the $\text{V}/(\text{V} + \text{Ni})$ ratio is positively related to the redox state of the sediment (Hatch and Leventhal 1992; Jones and Manning 1994; Li et al. 2018). In general, $\text{V}/(\text{V} + \text{Ni})$ values: < 0.6 indicate an oxygen-rich environment; between 0.6 and 0.84 indicate weak water stratification and anoxic/suboxide sedimentary environment; and > 0.84 suggest higher water stratification and an anaerobic environment (Zou et al. 2021). The $\text{V}/(\text{V} + \text{Ni})$ ratio values for the core SP9 are between 0.6 and 0.84, indicating weak water stratification and anoxic/suboxide sedimentary environment (Fig. 7). The $\text{V}/(\text{V} + \text{Ni})$ values in core SP9 are generally lower than in cores SP3, SP5, and SP6, indicating that the region is less prone to water column stratification and is not affected in general by such marked oxygen deficiency than other Sepetiba Bay areas as suggested for cores SP3 and SP5.

The variation in P-wave velocity indicates the presence of gas at relatively shallow levels in the sediments. P-wave velocities vary considerably along the core SP9 (255–1561 m s^{-1}). In subsurface marine sediments, the velocities of these waves are higher in sands (medium, fine and muddy sand) than in mud (e.g., Macedo et al. 2009): mean values around 1752 m s^{-1} are characteristic of medium sands. Values between 1492 and 1498 m s^{-1} were recorded in sandy mud and consolidated mud, respectively. P-wave velocities $< 800 \text{ m s}^{-1}$ have been measured in gas-saturated subsurface marine sediments and 4000 m s^{-1} in sedimentary rocks deposited in the deepest parts of a basin (Ayres Neto 2000). Thus, it can be assumed that the reduction in P-wave velocity between 100 and 56 cm depth in core SP9 may

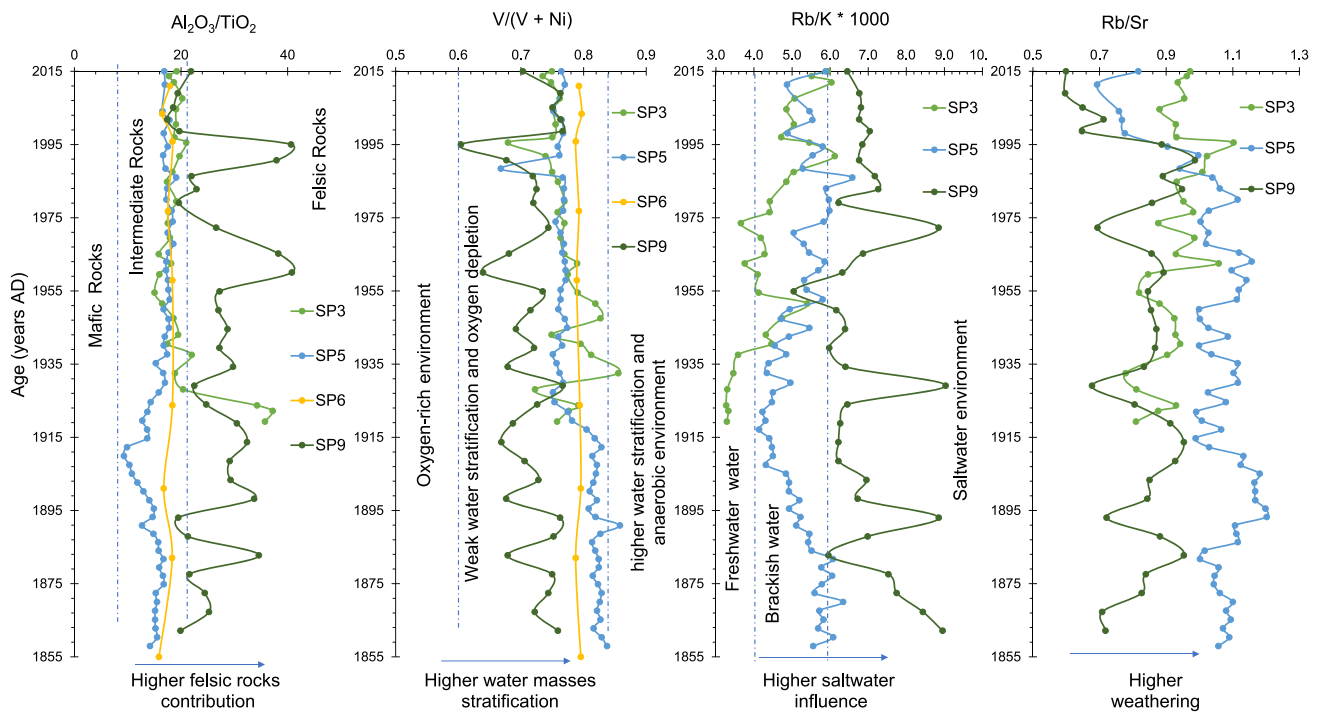


Fig. 7 Age plots of $\text{Al}_2\text{O}_3/\text{TiO}_2$, $\text{V}/(\text{V} + \text{Ni})$, Rb/K (*1000) and Rb/Sr ratios in cores SP9, SP3, SP5 and SP6. Dashed vertical lines mark boundaries explained in the text. Arrows at the bottom of the graphs mark trends

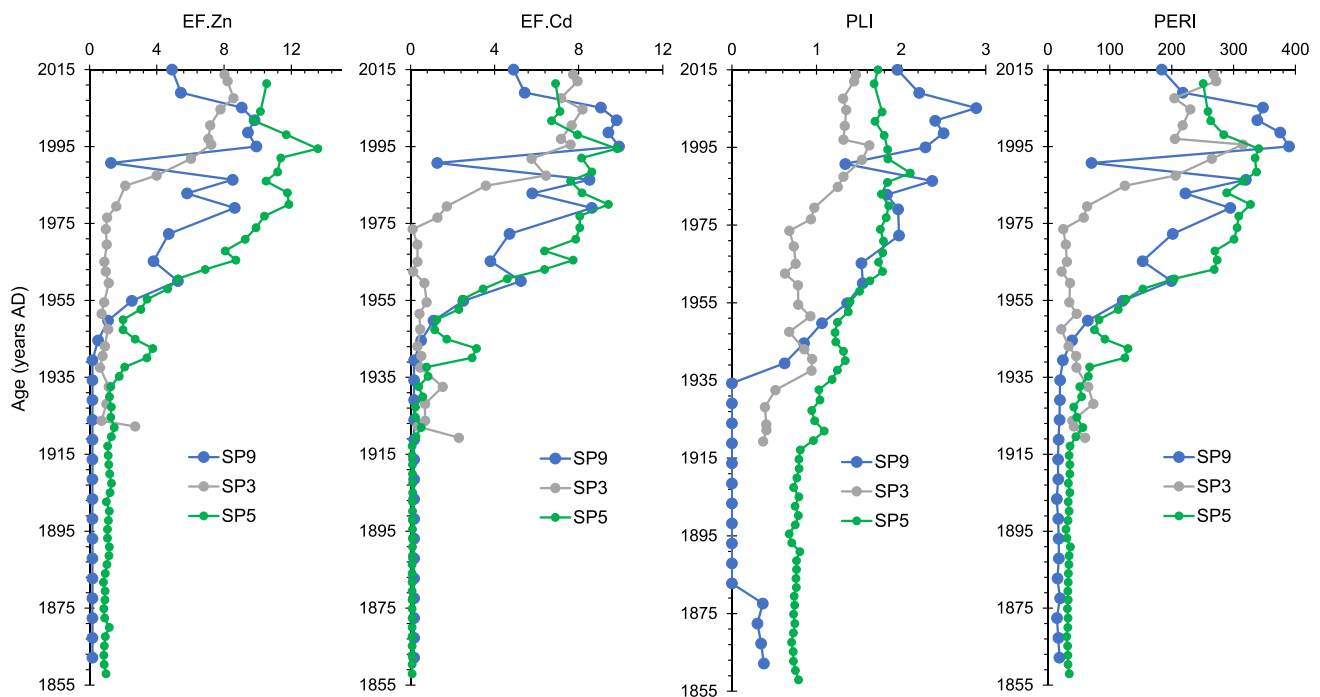
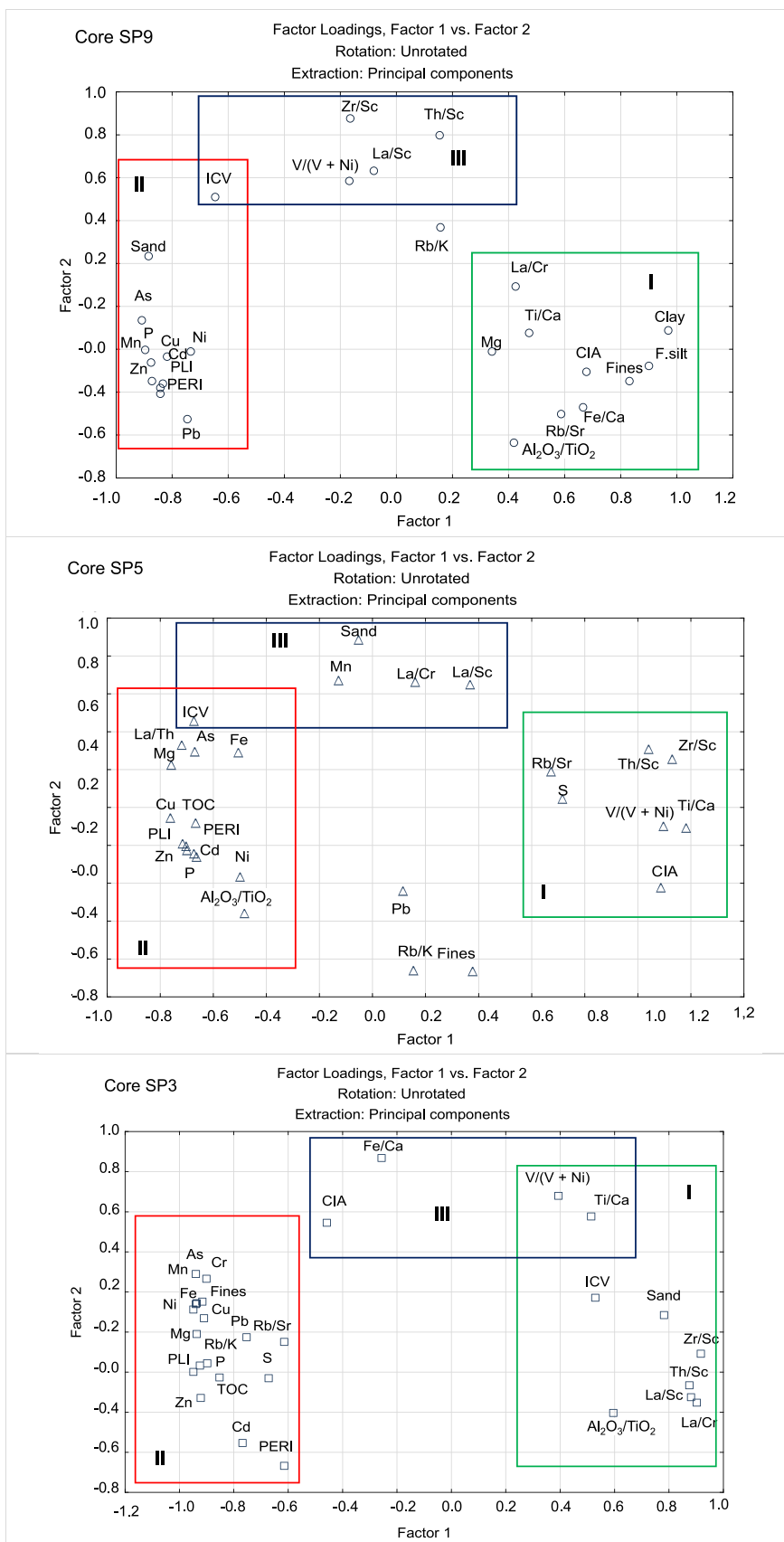


Fig. 8 Comparison of depth plots of EF values of Zn and Cd, PLI and PERI in core SP9 and cores SP3 (Castelo et al. 2021a, b) and SP5 (Silva et al. 2022a, b). Dots represent values

Fig. 9 Biplot of the two first principal components of the PCA based on selected grain size and geochemical variables for cores SP9, SP5, and SP3. Clay—clay fraction (<2 μm); F.silt—fine silt (2–8 μm); Sand—total sand and gravel fractions (> 63 μm); ICV—index of compositional variability; CIA—chemical index of alteration, PLI—Pollution Load Index; PERI—potential ecological risk index



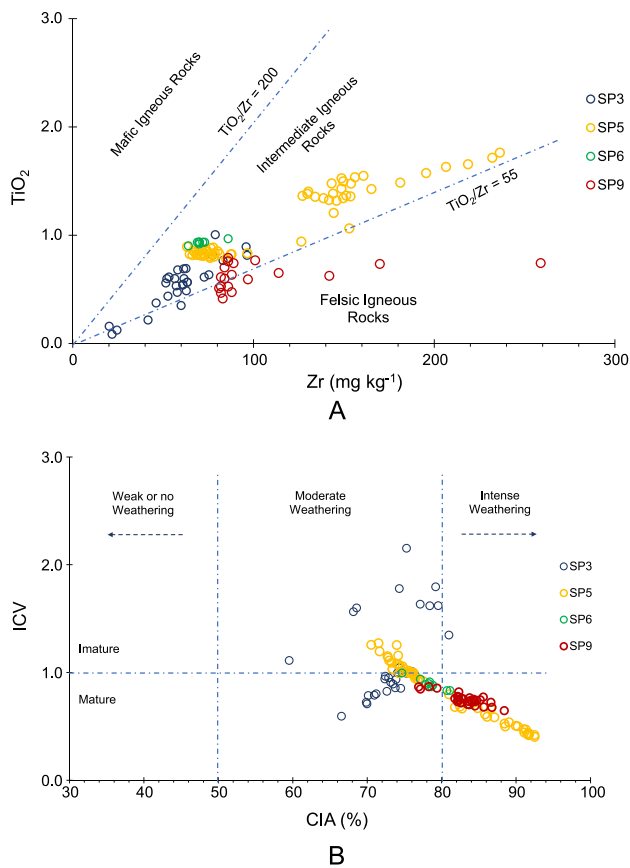


Fig. 10 Scatter plots obtained in core SP9 compared with that of cores SP3, SP5, and SP6. **A** Zr vs TiO_2 comparing results; the fields suggested by Hayashi et al. (1997) are represented in the figure to indicate possible sediment sources. **B** Chemical alteration index (CIA) vs index of chemical variability (ICV); fields defined considering Nesbitt and Young (1982) and Cox et al. (1995)

be related to the presence of gas in the sediment (Fig. 3). In cores SP12, SP13, and SP14 was also observed reduction in P-wave velocity in several subsurface levels, probably related to the presence of gas, due to the organic matter degradation by bacterial activity. Thus, the presence of gas is not only a local phenomenon but also may occur in some areas of Sepetiba Bay.

The sources of organic matter supplied to the sediments of core SP9 were analyzed from $\delta^{13}\text{C}$ and $\delta^{15}\text{N}$ values and the C/N ratio. The $\delta^{13}\text{C}$ values decrease systematically at the levels where TOC contents rise, and the sharpest decrease was observed at 1968 (42 cm level), corresponding to the maximum TOC peak (3.38%; Fig. 5); this trend is indicated by the significant negative correlations between TOC and $\delta^{13}\text{C}$ values (Appendix 4).

The C/N ratio value for organic matter has been used to trace the origin of organic matter (Emerson and Hedges 1988; Meyers 1994). According to these authors, the C/N ratios of organic matter from marine productivity is < 7;

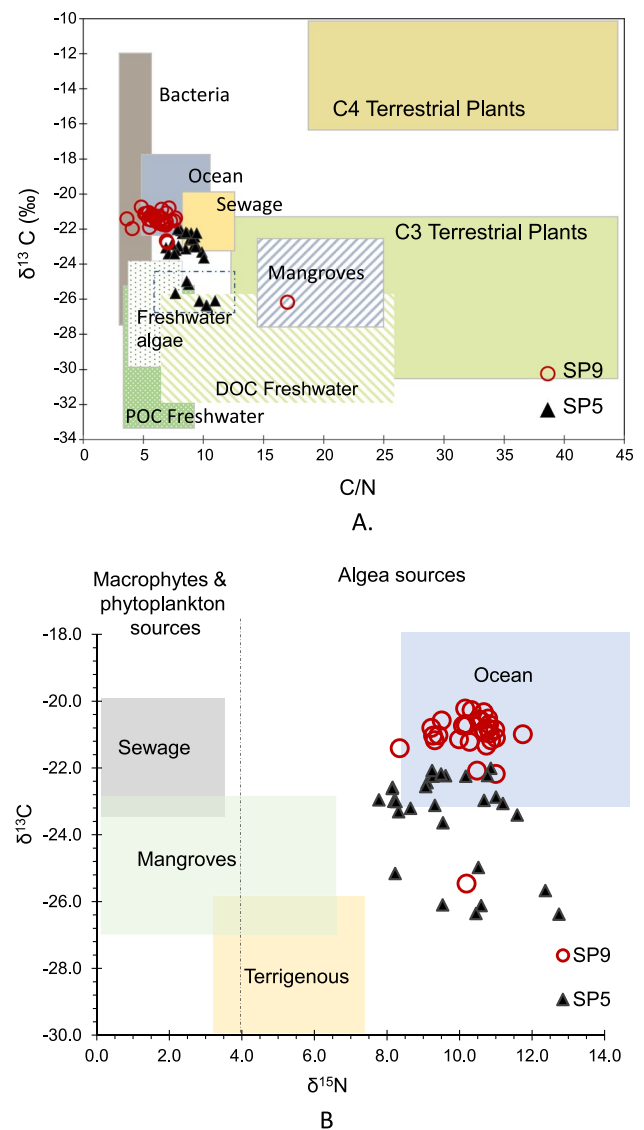


Fig. 11 Scatter plot of the values of **A** $\delta^{13}\text{C}$ vs C/N and; **B** $\delta^{13}\text{C}$ vs $\delta^{15}\text{N}$ in cores SP5 and SP9. In **A** the fields were marked according to Deines (1980), Lamb et al. (2006), Martinelli et al. (2009), Barros et al. (2010), and Bueno et al. (2019). DOC—dissolved organic carbon; POC—particulate organic carbon

organic matter from the sea and terrigenous (soil organic matter) vary between 8 and 20, and from the terrigenous origin is > 20. According to Meybeck (1982), the C/N ratio of algae/bacteria is 6.

Values of C/N < 7 were found intercalated along the core SP9 (Fig. 7; Appendix 3), which indicates that they should have received mostly an organic matter of marine productivity (algae/bacteria). In the remaining sediment layers, the C/N ratio values ranged from 7 to 17.9, probably resulting from organic matter supplied from various sources.

The biplots of $\delta^{13}\text{C}$ vs. C/N (Fig. 11A) and $\delta^{13}\text{C}$ vs. $\delta^{15}\text{N}$ (Fig. 11B) and the signed fields based on Deines (1980),

Lamb et al. (2006), Martinelli et al. (2009), Barros et al. (2010) and Bueno et al. (2019), also allow us to infer about the main sources of organic matter in core SP9. Their results also were compared to that of core SP5. While in core SP5, a more significant influence of sources related to freshwater algae and sewage discharge is recognized, in core SP9 (under the more substantial oceanic influence), the $\delta^{13}\text{C}$ values around -20‰ are mainly related to organic matter derived from ocean productivity and marine phytoplankton (Stein 1991). However, the influence of other sources, such as bacteria, mangroves, freshwater algae, and sewage discharge, was also identified in this core (Fig. 11A, B). In core SP9, for example, the 42 cm level (1968) contains primarily organic matter supplied by mangroves, which are abundant in the area; the 82 cm (1916) and 114 cm (1875) seem to receive more organic matter from freshwater algae; while the 2 cm (2011), 10 cm (2003), 34 cm (1981) and 102 cm (1890) layers may contain the significant contribution of bacterial organic matter (Fig. 11 A).

Thus, cyclical changes in the type of organic matter supplied to the study site are observed in these records. They may be related to climatic oscillations, hydrodynamic, or geomorphological changes that may have influenced the transport and deposition of organic matter in this region.

Paleosalinity variations

To identify paleosalinity variations in the study area, the Rb/K ratio was used. Since Rb contents are three orders of magnitude lower than K ones, the ratio is usually multiplied by 1000 to facilitate the values' reading and analyzing data representativeness (Zou et al. 2021). Within this context, the limit of 4 for Rb/K values has been proposed between freshwater environment (< 4) and brackish water environment (4–6), and values > 6 as indicators of the saltwater environment (Liu and Cao 1984).

According to the age plot of the Rb/K ratio, presented in Fig. 7: since 1855, saline waters have influenced the area of core SP9 more than the areas of cores SP3 and SP5 due to their proximity to the Guandú River outflow. However, the age plot of Rb/K (Fig. 7) for core SP9 shows cyclic decreases of this ratio, indicating phases of a more significant influence of brackish waters in this distal area of Sepetiba Bay.

The increase in Rb/K values generally correlates to the rise in $V/(V + \text{Ni})$ values; this indicates that the increase in brackish water influence in this region, probably caused by the augmented rainfall, may have contributed to the stratification of the water column; relatively high $V/(V + \text{Ni})$ values also may have been caused by higher fluxes of organic matter to the bottom and further reduction of oxygen content in the sediment due to its decomposition.

Periods of increased Rb/K values also indicate significant weathering and reduction of K-rich minerals. They coincide

with abrupt decreases in Rb/Sr values, indicating the presence of a greater abundance of Rb-associated minerals. During these periods, $\text{Al}_2\text{O}_3/\text{TiO}_2$ values decrease, denoting the deposition of sediments more enriched in mafic minerals and reducing feldspars, which also agrees with what was mentioned above.

Sediment pollution

Potentially toxic chemical elements such as Zn, Cd, Ni, Pb, Cu, and As show increasing trends from the bottom to the top of the core SP9 (Fig. 5). However, only Cd and Zn reach high CF and EF values (EF = 10; CF = 12/11; Appendix 3) indicating significant enrichment. According to the Brazilian regulation for dredging operations, only Cd and Zn exceed the threshold values established by CONAMA (2012) in core SP9.

According to the Igeo values, the upper layers of core SP9 are moderately to strongly polluted by Cd and Zn (Appendix 3). The RI values reveal high ecological risk by Cd. The PERI values show that the sediments from the top of the SP9 core have moderate to high ecological risk. The correlations of the PTEs with Mn indicate that they may be associated with Mn compounds, such as oxides and hydroxides.

The PLI values reveal a progressive increase in environmental degradation in this region of Sepetiba Bay. Cadmium and Zn contamination is known in Sepetiba Bay and has been studied by several authors (Barcellos et al. 1997; Araújo et al. 2017a, b; Morales et al. 2019a, b; Martins et al. 2019; Rodrigues et al. 2020; Castelo et al. 2021a, b; Silva et al. 2022a, b). With the accelerated urbanization and industrialization of the region, several industries and ports began to be installed around this bay (Patchineelam et al. 2011).

Human activity in the region is ancient and preceded colonization, which began in the early sixteenth century; the coast was then inhabited by the Tamoios, indigenous people from the Tupinambá nation (Duffy and Metcalf 2012). However, the history of industrial development in the Metropolitan Region of Rio de Janeiro has its most remarkable poignancy in the early 1940s, with the beginning of the construction of major highways such as Brazil Avenue (inaugurated in 1946) and the Presidente Dutra Highway, connecting the City of Rio de Janeiro to the City of São Paulo (inaugurated in 1951).

Created in 1967 by law 5969, the Companhia de Desenvolvimento Industrial do Estado do Rio de Janeiro was the main driver of the state's industrial development. A project for implementing industrial districts throughout the state was started from it. In the region near Sepetiba Bay, the industrial district of Santa Cruz was implemented near the Guandú River mouth, a project that was ongoing in the 1960s and started operating in 1975 (Codin 2017).

Other polluting industries also had their great importance in the increase of pollution in Sepetiba Bay, such as the opening in 1962 of the Ingá Mercantil Company in Madeira Island and the most recent implementation of the Companhia Siderúrgica do Atlântico in 2010 to transport all this raw material, it was necessary to build a port, initially called Port of Sepetiba, but later called Port of Itaguaí. Its construction started in 1976, and the bay dredging began in 1977. Its inauguration was in 1982, and its main objective was to serve the industrial complex of Santa Cruz (Portal do Governo Brasileiro 2023).

Metal contamination in the first half of the twentieth century was negligible (Fig. 8). However, the installation and operation of Ingá Mercantil Company, a galvanizing plant installed in Madeira Island between the 1962 and 1990s (Fig. 1), contributed to the significant degradation of Sepetiba Bay. This plant was a major producer of zinc in Brazil (60,000 t per year) obtained from silicate ores from Minas Gerais (Brazil). The zinc purification was inefficient and contributed to the high production of improperly stored waste (Barcellos and Lacerda 1994). The waste accumulation ($\approx 600,000$ t, containing ≈ 200 t of Cd and $\approx 50,000$ t of Zn) was exposed to the open air (Molisani et al. 2004). It was leached out during high rainfall events and contaminated surrounding areas, namely mangroves and the Sepetiba Bay (Molisani et al. 2004). The contamination recorded in core SP9 and cores SP3 and SP5 since the 1960s should be related to the environmental liabilities generated by this company and probably other industries in the area.

Factor 1 of the PCA (Fig. 9) explains geochemical parameters influenced by hydrodynamics. Contrary to what would be expected, the enrichment in PTEs (As, Cd, Ni, Pb, Cu, and Zn) in the study area is related to relatively coarse sediments. However, they are relatively enriched in organic carbon. Higher metal enrichment is generally observed in areas of calm sediment accumulation prone to the deposition of finer sediments enriched in organic matter. This rule is not observed in core SP9 since the highest concentrations of PTEs are associated with relatively coarse sediments.

On the other hand, the enrichment in PTEs is negatively correlated with lithogenic indicators such as Fe/Ca and Ti/Ca ratios, whose increase allows us to identify higher terrigenous input (Arz et al. 1998); Al_2O_3/TiO_2 , La/Cr and Th/Sc, whose increase indicates higher concentration in felsic particles. However, they are significant and positively associated with higher ICV values, whose increase indicates more significant compositional variability of the source rock (Cullers 2000; Armstrong-Altrin et al. 2015a, b; Ndjigui et al. 2018). These results suggest that the PTEs (As, Cd, Ni, Pb, Cu, and Zn) have followed a different distribution pattern of sedimentary dynamics and sediment deposition in the study area since the 1970s.

These metals' negative peaks were observed in the EF-Zn and EF-Cd values around 1988. It might be related to the reduced release of metals into Sepetiba Bay due to the containment dam construction around the perimeter of the Ingá Mercantil Company waste piles in 1984 (Ribeiro et al. 2015). However, the dam broke down in 1996, releasing high contents of PTEs into the bay (namely As, Cd, Pb, and Zn; Ribeiro et al. 2015). The structure of the containment dam began to deteriorate, and in 2003, the effluents were drained directly into the surrounding areas, contaminating the region's mangroves (Molisani et al. 2004). After 2005, the enrichment of Cd and Zn decreased due to the remediation of the discarded tailings (Gonçalves et al. 2020). It should be noted that the waste pile of the Ingá Mercantil Company was re-managed in 2012 (Araújo et al. 2017a, b). This history is represented mainly in the PTEs, EF-Cd, and EF-Zn values of core SP9 (Figs. 5, 8).

On the other hand, the EF-Zn values of core SP9, in comparison with those of cores SP3 and SP5, are the lowest until 1945. However, from that date onwards, they began to rise and approached the values observed in core SP5, located near the Ingá Mercantil company, the main source of the metals. The EF-Cd values of the core SP9 have a similar pattern but exceed those of the core SP3 (located in the central area of Sepetiba Bay) between 1986 and 2005.

Else, the PTE concentrations from core SP9 do not seem to be necessarily associated with sediments consisting of essentially felsic particles (as indicated, for example, by Al_2O_3/TiO_2 , La/Sc, and Zr/Sc ratios) but are found in levels with higher chemical variability, richer in mafic components (indicated by positive correlations with TiO_2/Zr). These characteristics are not typical of this shallow coastal area, undergoing constant wave and current reworking. Furthermore, the increased concentrations of PTEs are not correlated with the $V/(V + Ni)$ values, indicative of higher water mass stratification, and Rb/K values, tracing freshwater inflow in the area.

Notably, in the SP9 core, the PERI and PLI reach higher values than in core SP3 and are similar to SP5 (Fig. 8), which are closer to the polluting source area. It leads us to assume that the PTEs should be transported from distant areas (from the Madeira Island region) in events of high hydrodynamics by advection (Cunha et al. 2006) and strong bottom currents (Baptista Filho 2004) and from dredge spoil disposal areas. According to Lacerda et al. (2004), the sediments deposited in mangrove regions and mud tidal protected regions are also the most enriched by metals and show the highest accumulation rates of these metals. However, as core SP9 is close to dredging spoil disposal sites (1, 2, and 3; Fig. 1), likely, metal enrichment in this region is mainly a consequence of those activities. Dredging and deposition of dredged materials can cause turbulence, generate a turbid plume, increase the resuspension of sediments and facilitate

material dispersion (Cutroneo et al. 2012; Wasserman et al. 2013). This material is transported to the study area by tidal currents and retained by the Marambaia Barrier Island and the Ponta da Pombeba spit, giving place to high environmental degradation and ecological risk (indicated by PLI and PERI values).

The PCA biplot of factor 1 versus factor 2 for core SP3 shows a similar situation as for core SP9 (Fig. 9). Core SP3 is close to the dredge spoil disposal site 5 (Fig. 1). The PCA for core SP3 also places the PTEs in opposition to lithogenic indicators, in general, except CIA, but associates them with increased finer-grained sediments and TOC, as well as Rb/K and Mg values (more significant marine influence) and Rb/Sr (higher weathering) (Fig. 7). These data indicate that the turbid plumes of material dumped at site 5 are probably blocked by oceanic fronts. These fronts generate favorable conditions for the deposition of fines (including intensely weathered sediments), organic matter, and metals. PTEs end up being trapped in oxides and hydroxides of Mn or Fe sulfides, depending on the redox conditions of the sediment.

The PCA biplot of factor 1 versus factor 2 for core SP5 (Fig. 9) reveals a lesser influence of dredging activities in the area. The PCA for core SP5 suggests that metal enrichment is also associated with increasing organic matter and the deposition of immature sediments (indicated by ICV) consisting mainly of components supplied by intermediate igneous rocks (indicated by Al_2O_3/TiO_2 ratio; Fig. 7).

The possible influence of Ponta da Pombeba tip configuration

Factor 2 of the PCA (Fig. 9) is related to the more significant oceanic influence (Rb/K) and the weak stratification of the water masses (indicated by $V/(V+Ni)$ values) and the deposition of felsic sediments (traced by Th/Sc, La/Sc, and Zr/Sc) and other minerals but not clay minerals (see ICV values) in the study area. This factor represents coastal sediment dynamics. It shows cyclic increases in the oceanic influence in the study area (peaks of Rb/K; Fig. 7).

According to Reis et al. (2013, 2020) and Dadalto et al. (2021), the tidal channel features that were carved in the past (last glaciation, early Holocene) in this region where today Sepetiba Bay is located might have influenced the sediment transposition and conditioned the development stages of Ponta da Pombeba (erosion *versus* sandy strand deposition). Dadalto et al. (2021), using Ground Penetrating Radar (GPR) data and dating, described a model that shows distinct phases of Ponta da Pombeba development. These phases are well marked at the top of the sedimentary succession of the Marambaia Barrier Island and Ponta da Pombeba. Considering the location of core SP9, near the Ponta da Pombeba tip, an unstable structure whose length and configuration change temporally (Dadalto et al. 2021),

the Rb/K peaks (this work; Fig. 7) can be interpreted as an indirect indicator of the degradation phases of this spit. Stability in the Rb/K values after 1975 is probably related to a configuration of the Ponta da Pombeba tip similar to the present one (longer length; see Fig. 9 of Dadalto et al. 2021). It has facilitated the retention of PTEs, namely Cd and Zn, contributing to the degradation of the ecological quality of this region (indicated by PLI and PERI).

Main changes in environmental indicators that influenced the sedimentary evolution near Ponta da Pombeba since 1850

Because of the aspects presented here, it is clear that the integrated use of geophysical, textural, geochemical, and mineralogical proxies was of great value in understanding the action of both natural and anthropic processes in the distal region of Sepetiba Bay. The geochemical proxies used in comparison with those acquired in other cores (SP3, SP5, and SP6), collected in different areas of the inner zone of Sepetiba Bay, show that the SP9 is the core with a higher oceanic character, which would be expected given its location in the outer region of Sepetiba Bay.

Despite its distance from the sources of pollution, located onshore and Madeira Island, the SP9 core is located in the area of contamination plumes spreading in the bay. The results show that the area of the core SP9 has been undergoing a eutrophication process and is polluted by metals. The study of the variation of P waves in core SP9 allows us to infer the presence of gases retained in the sediment between the 100 and 56 cm depth horizons, produced probably by bacterial activity. This phenomenon is not only local. Sub-surface (biogenic) gas was also identified in cores SP12, SP13, and SP14 near Marambaia Barrier Island. This phenomenon still needs to be studied in the region and needs detailed research to know its true extent and impact on nature since the gas formed can be released into the atmosphere.

Nevertheless, the present and recent sedimentary cover in the shallow areas near Marambaia Barrier Island consists of sandy sediments aggraded by carbonates resulting from chemical precipitation by evaporitic processes, sometimes making hardened crusts. In core SP9, this process is represented by a significant increase in carbonate since 1975. However, other events of more intense evaporitic processes have been identified, e.g., around 1895. Although this type of sediment can block gas escape to the atmosphere, it also displays a significant organic matter content due to the high biological productivity that occurs within this ecosystem.

The geochemical proxies used in core SP9 indicate cyclic phenomena occurring since 1855 involving changes in the type of detrital sediment accumulation and the supply of organic matter and diagenetic processes occurring in the region. This cyclicity may be related to climatic oscillations,

changes in coastal sedimentary dynamics, and the geomorphology of the Ponta da Pombeba spit.

Core SP9 records events of lower salinity and stratification of the water masses indicated by the lower values of the Rb/K ratio in four periods caused by higher rainfall. The water circulation within the SB favored continental water transportation to more distant regions.

Nonetheless, the geochemical indicators suggest no relationship between these events and metal contamination in this sector of Sepetiba Bay. The sediment in this region is moderately to strongly polluted by Cd and Zn. It reaches degradation levels higher than those observed in areas closer to the decommissioned Ingá Mercantil Company. However, core SP9 is located near three disposal areas for dredged materials from the port region near Madeira Island (where Ingá Mercantil company was set). It can, therefore, be deduced that the main cause of contamination of this region is the turbid plumes formed when the dredged materials are deposited or the remobilization of sediments from the nearby disposal areas.

The geochemical proxies applied on core SP9 indicate the cyclic occurrence of more significant oceanic influence in this area. They may be related to changes in the extension and configuration of the Ponta da Pombeba spit. The recent extension of this structure associated with the presence of the Marambaia Barrier Island should have favored the accumulation of metals in the study area.

Conclusion

The results of core SP9, compared with others published in the literature, show that the studied region protected by Ponta da Pombeba and Marambaia Barrier Island is favorable to organic matter and metal retention. That enrichment occurred mainly since ≈ 1950 due to the industrial activity around Sepetiba Bay, as documented in several works.

This effect may have given rise to eutrophication phenomena, as it often happens in protected coastal environments. It may cause the presence of (biogenic) gas accumulated in shallow subsurface layers identified through geophysical data in core samples collected near Marambaia Barrier Island. The gas accumulation in this region, reported for the first time in this paper, was facilitated by evaporitic phenomena. These led to the formation of sediments hardened by the precipitation of carbonates, hindering the escape to the atmosphere of gases formed by bacterial activity in the subsurface sediments.

The results of this work show that the accumulation of PTEs since ≈ 1950 was not directly related to the sediments supplied to the study area through the coastal sedimentary dynamics. Disposal processes of contaminated

dredged spoils and dispersion of sediments from nearby industrial sites (current or past) and the configuration and extent of the Ponta da Pombeba spit and the presence of Marambaia Barrier Island (contributing to the reduction of current velocity and forming a metal retention barrier) were the leading causes of the ecological quality degradation of this distal region of Sepetiba Bay, since 1985.

This work is a poignant warning of the problems caused by the choice of sites to place the dredged spoils; in this case, due to the dispersion of polluted dredged spoils, pollutants were transferred to the distal region of Sepetiba Bay. Dredged spoils were dumped in nearby areas. The geomorphologic configuration of the area that conditions the circulation pattern of the oceanic currents has facilitated the retention of metals and organic matter in this region, heightening eutrophication and environmental degradation. Thus, this work shows the importance of conducting environmental impact studies before selecting sites for disposing of dredged materials in coastal regions.

Supplementary Information The online version contains supplementary material available at <https://doi.org/10.1007/s12665-023-11259-6>.

Acknowledgements This paper is a contribution of the projects of Conselho Nacional de Desenvolvimento Científico e Tecnológico of Brazil, CnPQ (project process # 443662/2018-5) and the Fundação de Amparo à Pesquisa do Estado do Rio de Janeiro—FAPERJ (Edital “PENSA RIO”, process # E-26/010.003024/2014 and Edital Projetos Temáticos no Estado do Rio de Janeiro—2021, process # E-26/211.278/2021). Virginia Martins would like to thank the CNPq (process #302676/2019-8) and FAPERJ for the research grants (process #202.927/2019 and process # E-26/200.333/2023). Antonio Tadeu dos Reis also thanks CNPq and FAPERJ for the research grants (process #309779/2021-9 and process #200.427/2023, respectively). The authors would like to thank the Fundação para a Ciência e a Tecnologia—FCT, Portugal (GeoBioTec funding UID/GEO/04035/2019; UIDB/04035/2020) for financial support.

Author contributions MBS: data acquisition; data curation; formal data analysis; writing—original draft. MVAM: conceptualization; methodology; data acquisition; data curation; formal data analysis; investigation; writing and editing the original draft; supervision, financial acquisition. JVG: writing—original draft, supervision, financial acquisition. RCLF: data acquisition; investigation; financial acquisition. FdCFS: data acquisition. TPD: data acquisition. THT: data acquisition; writing—original draft. PADLF: data acquisition. CGS: data acquisition. ATdR: writing—original draft, financial acquisition. DT: data acquisition; data curation. LCdS: investigation; writing—original draft. SB: investigation. MH: investigation. FR: investigation; financial acquisition.

Funding Open access funding provided by FCTIFCCN (b-on). Financing received from: Conselho Nacional de Desenvolvimento Científico e Tecnológico of Brazil, CnPQ—project process # 443662/2018-5 and # 302676/2019-8. Fundação de Amparo à Pesquisa do Estado do Rio de Janeiro—FAPERJ (Edital “PENSA RIO”, process # E-26/010.003024/2014 and Edital Projetos Temáticos no Estado do Rio de Janeiro—2021, process # E-26/211.278/2021 research grants process #202.927/2019, process # E-26/200.333/2023, process #309779/2021-9 and process #200.427/2023. Fundação para a

Ciência e a Tecnologia—FCT, Portugal (GeoBioTec funding UID/GEO/04035/2019; UIDB/04035/2020).

Data availability The data supporting this work are available in tables and as supplementary materials.

Declarations

Conflict of interest The authors declare that there are no conflicts of interest.

Ethical approval The authors followed the ethical standards.

Consent to participate Authors have consent to participate.

Consent to publish Authors have consent to publish.

Open Access This article is licensed under a Creative Commons Attribution 4.0 International License, which permits use, sharing, adaptation, distribution and reproduction in any medium or format, as long as you give appropriate credit to the original author(s) and the source, provide a link to the Creative Commons licence, and indicate if changes were made. The images or other third party material in this article are included in the article's Creative Commons licence, unless indicated otherwise in a credit line to the material. If material is not included in the article's Creative Commons licence and your intended use is not permitted by statutory regulation or exceeds the permitted use, you will need to obtain permission directly from the copyright holder. To view a copy of this licence, visit <http://creativecommons.org/licenses/by/4.0/>.

References

- Abubakar U, Usman MB, Bello AM, Garba TA, Hassan S (2019) Geochemical and palaeocurrent analysis of the Tertiary Kerri-Kerri formation in the Gongola sub-basin of the northern Benue trough Northeastern Nigeria: implications for provenance, tectonic setting, and palaeoweathering. *SN Appl Sci*. <https://doi.org/10.1007/s42452-019-1196-7>
- Aguiar VMC, Baptista Neto JA, Fonseca EM (2021) Assessment of bottom sediment quality in Niterói harbor (Brazil, South America) through ecological indexes concerning nutrients and trace metals. *Environ Sci Pollut Res* 28(44):1–14. <https://doi.org/10.1007/s11356-021-15173-x>
- Akkoca BD, Eriş KK, Çağatay MN, Biltekin D (2019) The mineralogical and geochemical composition of Holocene sediments from Lake Hazar, Elazığ, Eastern Turkey: implications for weathering, paleoclimate, redox conditions, provenance, and tectonic setting. *Turk J Earth Sci* 28:760–785. <https://doi.org/10.3906/yer-1812-8>
- Alvares CA, Stape JL, Sentelhas PC, de Moraes Gonçalves JL, Sparovek G (2013) Köppen's climate classification map for Brazil. *Meteorol Z* 22(6):711–728. <https://doi.org/10.1127/0941-2948/2013/0507>
- Alves Martins MV, Pereira E, Figueira RCL, Oliveira T, Pinto Simon AFS, Terroso D, Ramalho JCM, Silva L, Ferreira C, Gerales MC, Duleba W, Rocha F, Rodrigues MA (2019) Impact of eutrophication on benthic foraminifera in Sepetiba Bay (Rio de Janeiro State, SE Brazil). *J Sediment Environ* 4(4):480–500. <https://doi.org/10.12957/jse.2019.47327>
- Alves Martins MV, Hohenegger J, Martínez-Colón M, Frontalini F, Bergamashi S, Laut L, Belart P, Mahiques M, Pereira E, Rene Rodrigues R, Terroso D, Miranda P, Gerales MC, Villena HH, Reis T, Socorro OAA, Sousa SHM, Yamashita C, Rocha F (2020) Ecological quality status of the NE sector of the Guanabara Bay (Brazil): a case of living benthic foraminiferal resilience. *Mar Pollut Bull* 158:111–449. <https://doi.org/10.1016/j.marpolbul.2020.111449>
- Appleby PG (2001) Chronostratigraphic techniques in recent sediments. In: Last WM, Smol JP (eds) *Tracking environmental change using lake sediments volume 1: basin analysis, coring, and chronological techniques*. Kluwer Academic, Netherlands, pp 171–203
- Appleby PG (2008) Three decades of dating recent sediments by fallout radionuclides, a review. *Holocene* 18(1):83–93. <https://doi.org/10.1177/0959683607085598>
- Appleby PG, Oldfield F (1978) The calculation of lead-210 dates assuming a constant rate of supply of unsupported ^{210}Pb to the sediment. *Catena* 5(1):1–8. [https://doi.org/10.1016/S0341-8162\(78\)80002-2](https://doi.org/10.1016/S0341-8162(78)80002-2)
- Appleby PG, Oldfield F (1983) The assessment of ^{210}Pb data from sites with varying sediment accumulation rates. *Hydrobiologia* 103:29–35
- Appleby PG, Richardson N, Nolan PJ (1991) ^{241}Am dating of lake sediments. *Hydrobiologia* 214:35–42
- Araújo DF, Peres LGM, Yopez S, Mulholland DS, Machado W, Tonhá M, Garnier J (2017a) Assessing man-induced environmental changes in the Sepetiba Bay (Southeastern Brazil) with geochemical and satellite data. *CR Geosci* 349:290–298. <https://doi.org/10.1016/j.crte.2017.09.007>
- Araújo DF, Boaventura GR, Machado W, Viers J, Weiss D, Patchineelam SR, Ruiz I, Rodrigues APC, Babinski M, Dantas E (2017b) Tracing of anthropogenic zinc sources in coastal environments using stable isotope composition. *Chem Geol* 449:226–235. <https://doi.org/10.1016/j.chemgeo.2016.12.004>
- Argast S, Donnely TW (1987) The chemical discrimination of clastic sedimentary components. *J Sediment Res* 57(5):813–823. <https://doi.org/10.1306/212F8C6F-2B24-11D7-8648000102C1865D>
- Armstrong-Altrin JS (2015) Evaluation of two multidimensional discrimination diagrams from beach and deep-sea sediments from the Gulf of Mexico and their application to Precambrian clastic sedimentary rocks. *Int Geol Rev* 57:1446–1461. <https://doi.org/10.1080/00206814.2014.936055>
- Armstrong-Altrin JS, Lee YI, Verma SP, Ramasamy S (2004) Geochemistry of sandstones from the Upper Miocene Kudankulam Formation, southern India: implications for provenance, weathering, and tectonic setting. *J Sediment Res* 74:285–297. <https://doi.org/10.1306/082803740285>
- Armstrong-Altrin JS, Nagarajan R, Madhavaraju J, Rosalez-Hoz L, Lee YI (2013) Geochemistry of the Jurassic and upper Cretaceous shales from the Molango Region, Hidalgo, Eastern Mexico: implications of source-area weathering, provenance, and tectonic setting. *CR Geosci* 345:185–202. <https://doi.org/10.1016/j.crte.2013.03.004>
- Armstrong-Altrin JS, Machain-Castillo ML, Rosales-Hoz L, Carranza-Edwards A, Sanchez-Cabeza J, Ruiz-Fernández AC (2015a) Provenance and depositional history of continental slope sediments in the southwestern Gulf of Mexico unraveled by geochemical analysis. *Cont Shelf Res* 95:15–26. <https://doi.org/10.1016/j.csr.2015.01.003>
- Armstrong-Altrin JS, Nagarajan R, Balaram V, Natalhy-Pineda O (2015b) Petrography and geochemistry of sands from the Chachalacas and Veracruz beach areas, western Gulf of Mexico, Mexico: Constraints on provenance and tectonic setting. *J S Am Earth Sci* 64(1):199–216. <https://doi.org/10.1016/j.jsames.2015.10.012>
- Arthur MA, Sageman B (1994) Marine black shales: depositional mechanisms and environments of ancient deposits. *Annu Rev*

- Earth Planet Sci 22:499–551. <https://doi.org/10.1146/annurev.ea.22.050194.002435>
- Ayers JC, Watson EB (1993) Rutile solubility and mobility in supercritical aqueous fluids. *Contrib Miner Petrol* 114:321–330. <https://doi.org/10.1007/BF01046535>
- Ayres Neto A (2000) Uso da sísmica de reflexão de alta resolução e da sonografia na exploração mineral submarina. *Braz J Geophys* 18:3
- Baptista Filho LS (2004) Capítulo 5: Oceanografia Física. Caracterização Oceanográfica da Costa do Estado do Rio de Janeiro: Trecho I—Baía de Sepetiba. Relatório de Pesquisa da FAPERJ. Departamento de Oceanografia da Universidade do Estado do Rio de Janeiro, Rio de Janeiro, pp 41–81
- Barcellos C, Lacerda LD (1994) Cadmium and zinc source assessment in the Sepetiba Bay and basin region. *Environ Monit Assess* 29(2):183–199. <https://doi.org/10.1007/BF00546874>
- Barcellos C, Lacerda LD, Ceradini S (1997) Sediment origin and budget in Sepetiba Bay (Brazil)—an approach based on multi-elemental analysis. *Environ Geol* 32(2):203–209
- Barros GV, Martinelli LA, Oliveira Novais TM, Ometto JP, Zuppi GM (2010) Stable isotopes of bulk organic matter to trace carbon and nitrogen dynamics in an estuarine ecosystem in Babitonga Bay (Santa Catarina, Brazil). *Sci Total Environ* 408:2226–2232. <https://doi.org/10.1016/j.scitotenv.2010.01.060>
- Begy R, Timar-Gabor A, Somlai J, Cosma C (2011) A sedimentation study of St. Ana Lake (Romania) applying the 210Pb and 137Cs dating methods. *Geochronometria* 38(2):93–100. <https://doi.org/10.2478/s13386-011-0017-6>
- Birk S, Chapman D, Carvalho L, Spears BM, Andersen HE, Argillier C, Auer S, Baattrup-Pedersen A, Banin L, Beklioglu M, Bondar-Kunze E, Borja A, Branco P, Bucak T, Buijse AD, Cardoso AC, Couture R, Cremona F, de Zwart D, Feld CK, Ferreira MT, Feuchtmayr H, Gessner MO, Gieswein A, Globevnik L, Graeber D, Graf W, Gutiérrez-Cánovas C, Hanganu J, Iskin U, Järvinen M, Jeppesen E, Kotamäki N, Kuijper M, Lemm JU, Lu S, Solheim AL, Mischke U, Moe SJ, Nöges P, Nöges T, Ormerod SJ, Panagopoulos Y, Phillips G, Posthuma L, Pouso S, Prudhomme C, Rankinen K, Rasmussen JJ, Richardson J, Sagouis A, Santos JM, Schäfer RB, Schinegger R, Schmutz S, Schneider SC, Schilling L, Segurado P, Stefanidis K, Sures B, Thackeray SJ, Turunen J, Uyarra MC, Venohr M, Von der Ohe PC, Willby N, Hering D (2020) Impacts of multiple stressors on freshwater biota across spatial scales and ecosystems. *Nat Ecol Evol* 4(8):1060–1068. <https://doi.org/10.1038/s41559-020-1216-4>
- Brito GB, de Souza TL, Bressy FC, Moura CWN, Korn MGA (2012) Levels and spatial distribution of trace elements in macroalgae species from the Todos os Santos Bay, Bahia, Brazil. *Mar Pollut Bull* 10:2238–2244. <https://doi.org/10.1016/j.marpolbul.2012.06.022>
- Brugam RB (1978) Pollen indicators of land-use change in Southern Connecticut. *Quat Res* 9:349–362. [https://doi.org/10.1016/0033-5894\(78\)90038-8](https://doi.org/10.1016/0033-5894(78)90038-8)
- Buat-Menard P, Chesselet R (1979) Variable influence of the atmospheric flux on the trace metal chemistry of oceanic suspended matter. *Earth Planet Sci Lett* 42:398–411. [https://doi.org/10.1016/0012-821X\(79\)90049-9](https://doi.org/10.1016/0012-821X(79)90049-9)
- Bueno C, Figueira R, Ivanoff MD, Toldo Junior EE, Fornaro L, García-Rodríguez FG (2019) A multi proxy assessment of long-term anthropogenic impacts in Patos Lagoon, southern Brazil. *J Sediment Environ* 4(3):276–290. <https://doi.org/10.12957/jse.2019.44612>
- Carvalho LMV, Jones C, Leibman B (2003) The South Atlantic convergence zone: intensity, form, persistence, and relationships with intraseasonal to interannual activity and extreme rainfall. *J Clim* 17:88–108. [https://doi.org/10.1175/1520-0442\(2004\)017%3c0088:TSACZI%3e2.0.CO](https://doi.org/10.1175/1520-0442(2004)017%3c0088:TSACZI%3e2.0.CO)
- Carvalho BC, Dalbosco ALP, Guerra JV (2020) Shoreline position change and the relationship to annual and interannual meteorological conditions in Southeastern Brazil. *Estuar Coast Shelf Sci* 235:106582. <https://doi.org/10.1016/j.ecss.2020.106582>
- Castelo WFL, Alves Martins MV, Ferreira PAL, Figueira R, Costa CF, Fonseca LB, Bergamashi S, Pereira E, Terroso D, Pinto AFS, Simon MB, Socorro OAA, Frontalini F, Silva LC, Rocha F, Geraldês M, Guerra JG (2021a) Long-term eutrophication and contamination of the central area of Sepetiba Bay (SW Brazil). *Environ Monit Assess* 193:100. <https://doi.org/10.1007/s10661-021-08861-1>
- Castelo WFL, Alves Martins MV, Martínez-Colón M, Guerra JV, Dadalto TP, Terroso D, Soares MF, Frontalini F, Duleba W, Socorro OAA, Geraldês MC, Rocha F, Bergamaschi S (2021b) Disentangling natural vs. Anthropogenic induced environmental variability during the Holocene: Marambaia Cove, SW sector of the Sepetiba Bay (SE Brazil). *Environ Sci Pollut Res* 28:22612–22640. <https://doi.org/10.1007/s11356-020-12179-9>
- Codin (2017) Companhia de Desenvolvimento Industrial do Estado do Rio de Janeiro. Regulamento Interno dos Distritos Industriais
- CONAMA (Conselho Nacional do Meio Ambiente) (2004) Resolução nº 344, de 25 de março de 2004. Estabelece as diretrizes gerais e os procedimentos mínimos para a avaliação do material a ser dragado em águas jurisdicionais brasileiras, e dá outras providências
- CONAMA (Conselho Nacional do Meio Ambiente). Resolução nº 454 de (2012) Estabelece as diretrizes gerais e os procedimentos mínimos para a avaliação do material a ser dragado em águas jurisdicionais brasileiras, e dá outras providências. Diário Oficial da União Federativa do Brasil, Brasília
- Cox R, Lowe DR, Cullers RL (1995) The influence of sediment recycling and basement composition on evolution of mudrock chemistry in the south-western United States. *Geochim Cosmochim Acta* 59:2919–2940. [https://doi.org/10.1016/0016-7037\(95\)00185-9](https://doi.org/10.1016/0016-7037(95)00185-9)
- Cullers RL (2000) The geochemistry of shales, siltstones and sandstones of Pennsylvanian-Permian age, Colorado, USA: implications for provenance and metamorphic studies. *Lithos* 51(3):181–203. [https://doi.org/10.1016/S0024-4937\(99\)00063-8](https://doi.org/10.1016/S0024-4937(99)00063-8)
- Cunha CLN, Rosman PCC, Ferreira AP, Monteiro TCN (2006) Hydrodynamics and water quality models applied to Sepetiba Bay. *Cont Shelf Res* 26:1940–1953. <https://doi.org/10.1016/j.csr.2006.06.010>
- Cutroneo L, Castellano M, Pieracci A, Povero P, Tucci S, Capello M (2012) The use of a combined monitoring system for following a turbid plume generated by dredging activities in a port. *J Soils Sediments* 12:797–809. <https://doi.org/10.1007/s11368-012-0486-0>
- Dadalto TP, Carvalho BC, Guerra JV, Reis AT, Silva CG (2021) Holocene morpho-sedimentary evolution of Marambaia Barrier Island (SE Brazil). *Quat Res*. <https://doi.org/10.1017/qua.2021.43>
- Dantas M (2000) Geomorfologia do Estado do Rio de Janeiro. Ministério de Minas e Energia, Secretaria de Minas e Metalurgia, CPRM—Serviço Geológico do Brasil, Brasília. <https://doi.org/10.13140/RG.2.2.32582.57923>
- Davies JL (1964) A morphogenic approach to world shorelines. *Zeitschr Geomorphol* 8:127–142. <https://doi.org/10.1127/zfg/mortensen/8/1964/127>
- Deines P (1980) The isotopic composition of reduced organic carbon. In: Fritz P, Fontes JCH (eds) Handbook of environmental isotope geochemistry, vol 1. Elsevier Scientific Publishing Company, Amsterdam, pp 329–406
- Duffy EM, Metcalf AC (2012) The return of Hans Staden: a go-between in the Atlantic world. JHU Press, USA, pp 59–68 (ISBN 978-1-4214-0346-5)

- Emerson S, Hedges JI (1988) Processes controlling the organic carbon content of open ocean sediments. *Paleoceanography* 3:621–624. <https://doi.org/10.1029/PA003i005p00621>
- Fernandez GB, Pereira TG, Rocha TB, Maluf V, Moulton M, Oliveira Filho SR (2017) Classificação Morfológica das dunas costeiras entre o Cabo Frio e o Cabo Búzios, litoral do estado do Rio de Janeiro. *Rev Brasil Geomorfol* 18:595–622
- Ferreira AP, Moreira MDR (2015) Metals pollution status in surface sediments along the Sepetiba Bay Watershed, Brazil. *J Coast Zone Manage* 18:404. <https://doi.org/10.4172/2473-3350.1000404>
- Ferreira PAL, Siegle E, Schettini CAF, Mahiques MM, Figueira RCL (2015) Statistical validation of the model of diffusion-convection (MDC) of ^{137}Cs for the assessment of recent sedimentation rates in coastal systems. *J Radioanal Nucl Chem* 303:2059–2071. <https://doi.org/10.1007/s10967-014-3622-z>
- Figueira RCL, Tessler MG, De Mahiques MM, Fukumoto MM (2007) Is there a technique for the determination of sedimentation rates based on calcium carbonate content? A comparative study on the Southeastern Brazilian shelf. *Soils Found* 47(4):649–656. <https://doi.org/10.3208/sandf.47.649>
- Friederichs YL, Reis AT, Silva CG, Toulemonde B, Maia RMC, Guerra JV (2013) Arquitetura sísmica do Sistema fluvio-estuarino da Baía de Sepetiba preservado na estratigrafia rasa da plataforma adjacente, Rio de Janeiro, Brazil. *Braz J Geol* 43(1):998–1012. <https://doi.org/10.5327/Z2317-48892013000100011>
- Gabriel FA, Ferreira AD, Queiroz HM, Vasconcelos ALS, Ferreira TO, Bernardino AF (2021) Long-term contamination of the Rio Doce estuary as a result of Brazil's largest environmental disaster. *Perspect Ecol Conserv* 19(4):417–428. <https://doi.org/10.1016/j.pecon.2021.09.001>
- Geotek (2016a) Magnetic susceptibility. Available at <http://www.geotek.co.uk/products/magsusc>. Accessed February 2023
- Geotek (2016b) Non-contact resistivity. Available at <http://www.geotek.co.uk/products/ncr>. Accessed February 2023
- Gharibreza M, Raj J, Yusoff I, Othman Z, Tahir W, Ashraf M (2013) Sedimentation rates in Bera Lake (Peninsular Malaysia) using ^{210}Pb and ^{137}Cs radioisotopes. *Geosci J* 17(2):211–220. <https://doi.org/10.1007/s12303-013-0013-3>
- Godoy JM, Moreira I, Bragança MJ, Wanderley C, Mendes LB (1998) A study of Guanabara Bay sedimentation rates. *J Radioanal Nucl Chem* 227(1–2):157–160. <https://doi.org/10.1007/BF02386450>
- Goldich SS (1938) A study of rock weathering. *J Geol* 46:17–58. <https://doi.org/10.1086/624619>
- Gonçalves RA, Oliveira DF, Rezende CE, Almeida P, de Lacerda LD, da Gama BAP, Godoy JM (2020) Spatial and temporal effects of decommissioning a zinc smelter on the sediment quality of an estuary system: Sepetiba Bay Rio de Janeiro Brazil. *J Braz Chem Soc* 31(4):627–855. <https://doi.org/10.21577/0103-5053.20190232>
- Groot PA (2009). In: de Groot PA (ed) *Handbook of stable isotope analytical techniques*, vol 2. Elsevier, Amsterdam
- Håkanson L (1980) Ecological risk index for aquatic pollution control. A sedimentological approach. *Water Res* 14:975–1001. [https://doi.org/10.1016/0043-1354\(80\)90143-8](https://doi.org/10.1016/0043-1354(80)90143-8)
- Hatch JR, Leventhal JS (1992) Relationship between inferred redox potential of the depositional environment and geochemistry of the Upper Pennsylvanian (Missourian) Stark Shale Member of the Dennis Limestone, Wabaunsee County, Kansas, USA. *Chem Geol* 99(1–2–3):65–82
- Hayashi KI, Fujisawa H, Holland HD, Ohmoto H (1997) Geochemistry of ~1.9 Ga sedimentary rocks from northeastern Labrador, Canada. *Geochim Cosmochim Acta* 61:4115–4137. [https://doi.org/10.1016/S0016-7037\(97\)00214-7](https://doi.org/10.1016/S0016-7037(97)00214-7)
- Heilbron M, Eirado LG, Almeida J (Orgs) (2016) *Geologia e recursos minerais do Estado do Rio de Janeiro*. texto explicativo dos mapas geológico e de recursos minerais do Estado do Rio de Janeiro. Programa Geologia do Brasil—PGB/Coleção de mapas geológicos estaduais (Integração, atualização e difusão de dados da geologia do Brasil)
- Heilbron M, Machado N (2003) Timing of terrane accretion in the Neoproterozoic-Eopaleozoic Ribeira orogen (se Brazil). *Precamb Res* 125(1–2):87–112. [https://doi.org/10.1016/s0301-9268\(03\)00082-2](https://doi.org/10.1016/s0301-9268(03)00082-2)
- Jones B, Manning DAC (1994) Comparison of geochemical indices used for the interpretation of palaeo-redox conditions in ancient mudstones. *Chem Geol* 111(1):111–129. [https://doi.org/10.1016/0009-2541\(94\)90085-X](https://doi.org/10.1016/0009-2541(94)90085-X)
- Kamman NC, Engstrom DR (2002) Historical and present fluxes of mercury to Vermont and New Hampshire lakes inferred from ^{210}Pb dated sediment cores. *Atmos Environ* 36:1599–1609. [https://doi.org/10.1016/S1352-2310\(02\)00091-2](https://doi.org/10.1016/S1352-2310(02)00091-2)
- Khan NS, Ashe E, Shaw TA, Vacchi M, Walker J, Peltier WR, Kopp RE, Horton BP (2015) Holocene relative sealevel changes from near-, intermediate-, and far-field locations. *Curr Clim Change Rep* 1(4):247–262. <https://doi.org/10.1007/s40641-015-0029-z>
- Kjerfve B, Dias GTM, Filippo A, Gerald MC (2021) Oceanographic and environmental characteristics of a coupled coastal bay system: Baía de Ilha Grande-Baía de Sepetiba, Rio de Janeiro, Brazil. *Reg Stud Mar Sci* 41(2021):101594. <https://doi.org/10.1016/j.rsma.2020.101594>
- Koide M, Bruland KW, Goldberg ED (1973) Th-228/Th-232 and Pb-210 geo-chronologies in marine and lake sediments. *Geochim Cosmochim Acta* 37:1171–1187
- Kottek M, Grieser J, Beck C, Rudolf B, Rubel F (2006) World map of the Köppen–Geiger climate classification updated. *Meteorol Z* 15(3):259–263
- Krippner A, Meinhold G, Morton AC, Schöning J, Eynatten HV (2016) Heavy minerals and garnet geochemistry of stream sediments and bedrocks from the Almklovdalen area, Western Gneiss Region, SW Norway: implications for provenance analysis. *Sed Geol* 336:96–105. <https://doi.org/10.1016/j.sedgeo.2015.09.009>
- Kükre S, Erginal AE, Kılıç Ş, Bay O, Akarsu T, Öztura E (2020) Ecological risk assessment of surface sediments of Çardak Lagoon along a human disturbance gradient. *Environ Monitor Assessment* 192:359. <https://doi.org/10.1007/s10661-020-08336-9>
- Lacerda LD, Marins RV, Barcellos C, Molisani MM (2004) Sepetiba Bay: A case study of the environmental geochemistry of heavy metals in a subtropical coastal lagoon. *Environ Geochem Trop Subtrop Environ*. https://doi.org/10.1007/978-3-662-07060-4_21
- Lamb AL, Wilson GP, Leng MJ (2006) A review of coastal palaeo-climate and relative sea-level reconstructions using $\delta^{13}\text{C}$ and C/N ratios in organic material. *Earth Sci Rev* 75:29–57. <https://doi.org/10.1016/j.earscirev.2005.10.003>
- Lämmle L, Perez Filho A, Donadio C, Moreira VB, de Santos CJ, de Souza AO (2022) Baixos terraços marinhos associados às transgressões e regressões marinhas holocênicas na Planície Costeira do rio Paraíba do Sul Rio de Janeiro Brasil. *Rev Brasil Geomorfol* 23(2):1285–1303. <https://doi.org/10.20502/rbg.v23i2.1992>
- Leal Neto AD, Legey LFL, González-Araya MC et al (2006) A system dynamics model for the environmental management of the Sepetiba Bay Watershed, Brazil. *Environ Manage* 38:879–888. <https://doi.org/10.1007/s00267-005-0211-5>
- Li Y, Qu X, Zhang M, Peng W, Yu Y, Gao B (2018) Anthropogenic impact and ecological risk assessment of thallium and cobalt in Poyang Lake using the geochemical baseline. *Water* 10(11):1703. <https://doi.org/10.3390/w10111703>
- Long X, Yuan C, Sun M, Xiao W, Wang Y, Cai K, Jiang Y (2012) Geochemistry and Nd isotopic composition of the early Paleozoic flysch sequence in the Chinese Altai, Central Asia: evidence for a northward-derived mafic source and insight into model ages in









- an accretionary orogen. *Gondwana Res* 22:554–566. <https://doi.org/10.1016/j.gr.2011.04.009>
- Lürling M, Mucci M (2020) Mitigating eutrophication nuisance: in-lake measures are becoming inevitable in eutrophic waters in the Netherlands. *Restor Eutrophic Lakes* 847:4447–4467. <https://doi.org/10.1007/s10750-020-04297-9>
- Macedo HC, Figueiredo AG Jr, Machado JC (2009) Propriedades acústicas (velocidade de propagação e coeficiente de atenuação) de sedimentos marinhos coletados nas proximidades da Ilha do Cabo Frio, RJ. *Rev Brasil Geofís* 27(2):195–204
- Macedo GR, Pimentel RF (2004) Conflito e Integração na Transposição de Águas do Rio Paraíba do Sul para o Guandú. <http://www.producao.uff.br/conteudo/rpep/volume42004/publicacao2004.htm>. Accessed Nov 2023
- Martinelli LP, Ometto JPHB, Ferraz ES, Victoria RL, Camargo PB, Moreira MZ (2009). Desvendando Questões Ambientais com Isótopos Estáveis [Unraveling environmental issues with stable isotopes.]. Oficina de Textos, São Paulo
- Martins V, Dubert J, Jouanneau J-M, Weber O, Silva EF, Patinha C, Alveirinho Dias JM, Rocha F (2007) A multiproxy approach of the Holocene evolution of shelf–slope circulation on the NW Iberian continental shelf. *Mar Geol* 239:1–18. <https://doi.org/10.1016/j.margeo.2006.11.001>
- Martins MVA, Pereira E, Figueira RCL, Oliveira T, Simon AFSP, Terroso D, Ramalho JCM, Silva L, Ferreira C, Geraldês MC, Duleba W, Rocha F, Rodrigues MA (2019) Impact of eutrophication on benthic foraminifera in Sepetiba Bay (Rio de Janeiro State, SE Brazil). *J Sediment Environ* 4(4):480–500. <https://doi.org/10.12957/jse.2019.47327>
- Matsumoto E (1975) ^{210}Pb geochronology of sediments from Lake Shinji. *Geochem J* 9:167–172. <https://doi.org/10.2343/geochemj.9.167>
- McLennan SM, Hemming S, McDaniel DK, Hanson GN (1993) Geochemical approaches to sedimentation, provenance, and tectonics. *Geol Soc Am Spec Pap* 284:21–40. <https://doi.org/10.1130/SPE284-p21>
- Meybeck M (1982) Carbon, nitrogen, and phosphorous transport by world rivers. *Am J Sci* 282:401–450. <https://doi.org/10.2475/ajs.282.4.401>
- Meyers PA (1994) Preservation of elemental and isotopic source identification of sedimentary organic matter. *Chem Geol* 114:289–302. [https://doi.org/10.1016/0009-2541\(94\)90059-0](https://doi.org/10.1016/0009-2541(94)90059-0)
- Misumi S, de Barros M, Vilela C, Barth O (2014) Palinologia, Paleoflorística e Aspectos Paleoclimáticos de Sedimentos do Pleistoceno Tardio na Bacia Hidrográfica do Rio Guandú, Rio de Janeiro, Brasil. *Anuario do Instituto de Geociencias*, p 37. https://doi.org/10.11137/2014_1_104_114
- Molisani MM, Marins RV, Machado W, Paraquetti HHM, Bidone ED, Lacerda LD (2004) Environmental changes in Sepetiba Bay, SE Brazil. *Reg Environ Change* 4:17–27. <https://doi.org/10.1007/s10113-003-0060-9>
- Montezuma PN (2012) Análise de prováveis fatores causadores do processo de assoreamento na Baía de Sepetiba-RJ. Bacia hidrográfica dos Rios Guandú, da Guarda e Guandú-Mirim, INEA, Rio de Janeiro
- Morales SJD, Guerra JV, Nunes MAS, Alves Martins MV, Souza AM, Geraldês MC (2019a) Anthropogenic impacts on the western sector of Sepetiba Bay (SE Brazil) accessed by isotope composition of surface sediments. *J Sediment Environ* 4(3):291–311. <https://doi.org/10.12957/jse.2019.45269>
- Morales SJD, Guerra JV, Nunes MAS, de Souza AM, Geraldês MC (2019) Evaluation of the environmental state of the western sector of Sepetiba Bay (SE Brazil): trace metal contamination. *J Sediment Environ* 4(2):174–188. <https://doi.org/10.12957/jse.2019.43764>
- Müller VG (1986) Schadstoffe in sedimenten—Sedimente als Schadstoffe. *Mitt Osterr Geol Ges* 79:107–126
- Nagarajan R, Armstrong-Altrin JS, Kessler FL, Jong J (2017) Petrological and geochemical constraints on provenance, paleoweathering, and tectonic setting of clastic sediments from the Neogene Lambir and Sibuti Formations, northwest Borneo. In: Mazumder R (ed) *Sediment provenance influences on compositional change from source to sink*. Elsevier Inc., New York, pp 123–153
- Nascimento JR, Bidone ED, Rolão-Araripe D, Keunecke KA, Sabadini-Santos E (2016) Trace metal distribution in white shrimp (*Litopenaeus schmitti*) tissues from a Brazilian coastal area. *Environ Earth Sci* 75:990–998. <https://doi.org/10.1007/s12665-016-5798-8>
- Nascimento DN, Salomão MS, Mane MA, Geraldês MC, Alves Martins MV (2019) Marine Progression records in the Sepetiba Bay region (RJ-Brazil) by GPR and ground magnetic survey. *J Sediment Environ* 4(4):518–539
- Ndjigui PD, Onana VL, Sababa E, Bayiga EC (2018) Mineralogy and geochemistry of the Lokoundje alluvial clays from the Kribi deposits, Camaroonian Atlantic coast: implications for their origin and depositional environment. *J Afr Earth Sc* 143:102–117. <https://doi.org/10.1016/j.jafrearsci.2018.03.023>
- Nesbitt HW, Young GM (1982) Early proterozoic climates and plate motions inferred from major element chemistry of lutites. *Nature* 299:715–717. <https://doi.org/10.1038/299715a0>
- Netto AA, da Lima LS, Vieira KS, de Delgado JF, de Souza PF, Correa TR, Neto JAB, Gaylarde CC, da Fonseca EM (2022) Pollutants potential mobilization in Santos Bay/Brazil: subsidies for the environmental management of a highly anthropized estuary: Potencial de mobilização de poluentes na baía de Santos/Brasil: subsídios para a gestão ambiental de um estuário altamente antropizado. *Braz J Dev* 8(12):80834–80864
- Nunes M, Alves Martins MV, Frontalini F, Bouchet VMP, Francescangeli F, Hohenegger J, Figueira R, Senez-Mello TM, Castelo WFL, Damasceno FL, Laut L, Duleba W, Mello e Sousa SH, Antoniolli L, Geraldês MC (2023) Inferring the ecological quality status based on living benthic foraminiferal indices in transitional areas of the Guanabara Bay (SE Brazil). *Environ Pollut* 320(1):121003. <https://doi.org/10.1016/j.envpol.2023.121003>
- Ohr M, Halliday AN, Peacor DR (1991) Sr and Nd isotopic evidence for punctuated clay diagenesis. *Texas Gulf Coast. Earth Planet Sci Lett* 105:110–126
- Patchineelam SM, Sanders CJ, Smoak JM, Zem RC, Oliveira G, Patchineelam SR (2011) A historical evaluation of anthropogenic impact in coastal ecosystems by geochemical signatures. *J Braz Chem Soc* 22:120–125
- Pennington W, Cambray RS, Fisher EMR (1973) Observations on lake sediments using fallout ^{137}Cs as a tracer. *Nature* 242:324–326. <https://doi.org/10.1038/242324a0>
- Pereira SD, Santos SB (2012) Restos de moluscos na Baía de Sepetiba como indicadores de alterações pretéritas da linha de costa no Holoceno. In: da Rodrigues MAC, Pereira SD, dos Santos SB (Org) *Baía de Sepetiba: Estado da Arte*, 1st edn. Corbã, Rio de Janeiro, pp 105–111
- Pereira SD (1998) Influência da variação relativa do nível do mar no manguezal de Guaratiba—Baía de Sepetiba—RJ. Tese de Doutorado. Centro de Geologia Costeira e Oceânica, UFRGS, 133 p
- Perez Filho A, Rubira FG (2019) Evolutionary interpretation of Holocene landscapes in eastern Brazil by optimally stimulated luminescence: surface coverings and climatic pulsations. *Catena* 172:866–876. <https://doi.org/10.1016/j.catena.2018.06.031>
- Pinto AFS, Ramalho JCM, Borghi L, Carelli TG, Plantz JB, Pereira E, Terroso D, Santos WH, Geraldês MC, Rocha F, Rodrigues MAC, Laut L, Martins MVA (2019) Background concentrations of chemical elements in Sepetiba Bay SE Brazil. *J Sediment Environ* 4:108–123. <https://doi.org/10.12957/jse.2019.40992>

- Portal do Governo Brasileiro (2023). <https://www.portosrio.gov.br/pt-br/portos/porto-de-itaguaui/historia>. Accessed Oct. 2023
- Potratz GI, Geraldles MC, Bizzi S, Nogueira L, Alves Martins MV (2019) Using lead isotopes and potentially toxic elements to trace pollutant sources in the northern region of Guanabara Bay, south-eastern Brazil. *Mar Pollut Bull* 144:216–223. <https://doi.org/10.1016/j.marpolbul.2019.04.057>
- Protano C, Zinnà L, Giampaoli S et al (2014) Heavy metal pollution and potential ecological risks in rivers: a case study from Southern Italy. *Bull Environ Contam Toxicol* 92:75–80. <https://doi.org/10.1007/s00128-013-1150-0>
- Reis AT, Maia RM, Silva CG, Rabineau M, Guerra JV, Gorini C, Ayres A, Arantes-Oliveira R, Benabdellouahed MA, Simões IV, Tardin R (2013) Origin of step-like and lobate seafloor features along the continental shelf off Rio de Janeiro State, Santos Basin-Brazil. *Geomorphology* 203:25–45. <https://doi.org/10.1016/j.geomorph.2013.04.037>
- Reis AT, Amendola G, Dadalto TP, Silva CG, Poço RGTC, Guerra JV, Martins V, Rebouças RC, Gorini C, Rabineau M (2020) Arquitetura e Evolução Depositional da Sucessão Sedimentar Pleistoceno Tardio-Holoceno (últimos ~20 Ka) da Baía de Sepetiba (RJ). *Geociências* 39:695. <https://doi.org/10.5016/geociencias.v39i03.14366>
- Ribeiro AP, Figueiredo ANG, dos Santos JO, Ferreira PAL, Graudenz GS, Ruiz MS, de Mahiques MM, Figueira RCL, Wasserman JCFA (2015) Effects of contamination with toxic metals on the environmental quality of Sepetiba Bay (SE Brazil): the case of Ingá Company. *Manage Environ Qual* 26(4):538–555. <https://doi.org/10.1108/MEQ-06-2013-0074>
- Robbins JA, Edgington DN (1975) Determination of recent sedimentation rates in Lake Michigan using Pb-210 and Cs-137. *Geochim Cosmochim Acta* 39:285–304
- Rodrigues SK, Machado W, Guerra JV, Geraldles M, Morales S, Vinzón SB (2020) Changes in Cd and Zn distribution in sediments after closure of an electroplating industry, Sepetiba Bay, Brazil. *Mar Pollut Bull* 161:111758. <https://doi.org/10.1016/j.marpolbul.2020.111758>
- Rodríguez-Espinosa PF, Shruti VC, Jonathan MP, Martínez-Tavera E (2018) Metal concentrations and their potential ecological risks in fluvial sediments of Atoyac River Basin, Central Mexico: volcanic and anthropogenic influences. *Ecotoxicol Environ Saf* 148:1020–1033. <https://doi.org/10.1016/j.ecoenv.2017.11.068>
- Roncarati H, Carelli SG (2012) Considerações sobre o estado da arte dos processos geológicos cenozóicos atuantes na Baía de Sepetiba. *Baía de Sepetiba Estado da Arte*, Cap. 1, Rede BRASPOR
- Roser BP, Korsch RJ (1986) Determination of tectonic setting of sandstone mudstone suites using SiO₂ content and K₂O/Na₂O ratio. *J Geol* 94(635):650. <https://doi.org/10.1086/629071>
- Sabaris TPP, Bonotto DM (2011) Sedimentation rates in Atibaia River basin, São Paulo State, Brazil, using ²¹⁰Pb as geochronometer. *Appl Radiat Isot* 69(1):275–288. <https://doi.org/10.1016/j.apradiso.2010.08.016>
- Schön JH (1996) Physical properties of rocks. Fundamentals and principles of petrophysics. In: *Handbook of geophysical exploration*, section I, seismic exploration, vol 18. Pergamon Press, UK
- SEMADS (Secretaria de Estado de Meio Ambiente e Desenvolvimento Sustentável) (2001) In: Alves JRP (Org) *Manguezais: educar para proteger*. FEMAR: SEMADS, Rio de Janeiro, 96 p
- Shukla BS, Joshi SR (1989) An evaluation of the CIC Model of Pb dating. *Environ Geol Water Sci* 11:73–76. <https://doi.org/10.1007/BF01740587>
- Silva LC, Alves Martins MV, Castelo WFL, Saibro MB, Rangel D, Pereira E, Bergamaschi S, Sousa SHM, Varela J, Frontalini F, Chaves H, Reis AT, Aguilera O, Zaaboub N, Cheriyan E, Geraldles MC (2022a) Trace metals enrichment and potential ecological risk in sediments of the Sepetiba Bay (Rio de Janeiro, SE Brazil). *Mar Pollut Bull* 177:113485. <https://doi.org/10.1016/j.marpolbul.2022.113485>
- Silva LC, Alves Martins MV, Figueira R, Frontalini F, Pereira E, Senez-Mello TM, Castelo WFL, Saibro MB, Francescangeli F, Mello E, Sousa SH, Bergamaschi S, Antonioli L, Bouchet VMP, Terroso D, Rocha F (2022b) Unraveling anthropocene paleoenvironmental conditions combining sediment and foraminiferal data: proof-of-concept in the Sepetiba Bay (SE, Brazil). *Front Ecol Evol* 10(852439):2022. <https://doi.org/10.3389/fevo.2022.852439>
- Souza AO, Perez Filho A, Lämmle L, Souza DH (2020) Holocene climate pulses and structural controls on the geomorphological estuarine evolution of The Iguape River, São Paulo, Brazil. *Continent Shelf Res* 205:104168. <https://doi.org/10.1016/j.csr.2020.104168>
- Souza AM, Rocha DS, Guerra JV, Cunha BA, Martins MVA, Geraldles MC (2021) Metal concentrations in marine sediments of the Rio de Janeiro Coast (Brazil): a proposal to establish new acceptable levels of contamination. *Mar Pollut Bull* 165:112113. <https://doi.org/10.1016/j.marpolbul.2021.112113>
- Stein R (1991) Accumulation of organic carbon in marine sediments. Results from the DSDP/ODP. Springer-Verlag, Berlin, p 217
- Stumm W, Morgan JJ (1981) *Aquatic chemistry: an introduction emphasizing chemical equilibria in natural waters*. Wiley, New Jersey
- Sutherland RA (2000) Bed sediment-associated trace metals in an urban stream, Oahu, Hawaii. *Environ Geol* 39:611–627. <https://doi.org/10.1007/s002540050473>
- Swarnalatha K, Letha J, Ayoob S, Sheela AM (2013) Identification of silicon (Si) as an appropriate normalizer for estimating the heavy metals enrichment of an urban lake system. *J Environ Manage* 129:54–61. <https://doi.org/10.1016/j.jenvman.2013.05.039>
- Taylor SR, McLennan SM (1985) *The continental crust: its composition and evolution. An examination of the geochemical record preserved in sedimentary rocks*. Blackwell Science, Oxford, p 312
- Tian Y, Jiang Y, Liu Q, Dong M, Xu D, Liu Y, Xia X (2019) Using a water quality index to assess the water quality of the upper and middle streams of the Luanhe River, northern China. *Sci Total Environ* 667:142–151. <https://doi.org/10.1016/j.scitotenv.2019.02.356>
- Tomlinson DL, Wilson JG, Harris CR et al (1980) Problems in the assessment of heavy-metal levels in estuaries and the formation of a pollution index. *Helgolander Meeresun* 33:566–575. <https://doi.org/10.1007/BF02414780>
- Tubbs Filho D, Antunes JCO, Vettorazzi (Org.) JS (2012) *Bacia Hidrográfica dos rio Guandú, da Guarda e Guandú-Mirim—Experiências para a gestão dos recursos hídricos*, 1st edn. INEA, Rio de Janeiro
- Tupinambá M, Teixeira W, Heilbron M (2000) Neoproterozoic Western Gondwana assembly and subduction-related plutonism: the role of the Rio Negro Complex in the Ribeira Belt, South-eastern Brazil. *Rev Brasil Geociênc* 30:7–11
- Vieira KS, Baptista Neto JA, Crapez MAC, Gaylarde C, Pierri BS, Saldaña-Serrano M, Bainy ACD, Nogueira DJ, Fonseca EM (2021) Occurrence of microplastics and heavy metals accumulation in native oysters *Crassostrea Gasar* in the Paranaguá estuarine system, Brazil. *Mar Pollut Bull* 166:112225. <https://doi.org/10.1016/j.marpolbul.2021.112225>
- Vilela CG, Figueira BO, Macedo MC, Baptista Neto JA (2014) Late holocene evolution and increasing pollution in Guanabara Bay, Rio de Janeiro, SE Brazil. *Mar Pollut Bull* 79:175–187. <https://doi.org/10.1016/j.marpolbul.2013.12.020>
- Wang H, Ni J, Song Q, Li C, Wang F, Cao Y (2021) Analysis of coastal groundwater hydrochemistry evolution based on groundwater

- flow system division. *J Hydrol* 601:126631. <https://doi.org/10.1016/j.jhydrol.2021.126631>
- Wasserman JC, Barros S, Lima G (2013) Planning dredging services in contaminated sediments for balanced environmental and investment costs. *J Environ Manage* 121:48–56. <https://doi.org/10.1016/j.jenvman.2013.02.024>
- Wedepohl KH (1969) *Handbook of geochemistry*, vol 1. Springer-Verlag, Berlin Heidelberg, p 242
- Yuan GL, Sun TH, Han P, Li J, Lang XX (2014) Source identification and ecological risk assessment of heavy metals in topsoil using environmental geochemical mapping: typical urban renewal area in Beijing, China. *J Geochem Explor* 136:40–47. <https://doi.org/10.1016/j.gexplo.2013.10.002>
- Zaid SM, Gahtani FA (2015) Provenance, diagenesis, tectonic setting and geochemistry of Hawkesbury sandstone (Middle Triassic), southern Sydney Basin, Australia. *Turk J Earth Sci* 24:72–98. <https://doi.org/10.3906/yer-1407-5>
- Zheng X-J, Chen M, Wang J-F, Li F-G, Yan Y, Liu Y-C (2020) Ecological risk assessment of heavy metals in the vicinity of tungsten mining areas, Southern Jiangxi Province, soil and sediment contamination. *An Int J* 29(6):665–679. <https://doi.org/10.1080/15320383.2020.1763912>
- Ziemniak SE, Jones ME, Combs KES (1993) Solubility behavior of titanium (IV) oxide in alkaline media at elevated temperatures. *J Solution Chem* 22:601–623. <https://doi.org/10.1007/BF00646781>
- Zou C, Mao L, Tan Z, Zhou L, Liu L (2021) Geochemistry of major and trace elements in sediments from the Lubei Plain, China: Constraints for paleoclimate, paleosalinity, and paleoredox environment. *J Asian Earth Sci* 6(2021):100071. <https://doi.org/10.1016/j.jaesx.2021.100071>

Publisher's Note Springer Nature remains neutral with regard to jurisdictional claims in published maps and institutional affiliations.

Authors and Affiliations

Murilo Barros Saibro¹  · Maria Virgínia Alves Martins^{1,2}  · Josefa Varela Guerra³  · Rubens Cesar Lopes Figueira⁴  · Felipe de Castro Figueiredo Simões³ · Tatiana Pinheiro Dadalto⁵ · Tailisi Hoppe Trevizani⁴  · Paulo Alves de Lima Ferreira⁴ · Cleverson Guizan Silva⁶ · Antônio Tadeu dos Reis³  · Denise Terroso² · Layla Cristine da Silva¹  · Sergio Bergamaschi¹ · Fernando Rocha²  · Monica Heilbron¹

✉ Maria Virgínia Alves Martins
virginia.martins@ua.pt

Murilo Barros Saibro
murilosaibro@id.uff.br

Josefa Varela Guerra
josefa@uerj.br

Rubens Cesar Lopes Figueira
rfigueira@usp.br

Felipe de Castro Figueiredo Simões
felipe.simoes@uerj.br

Tatiana Pinheiro Dadalto
tatiana.dadalto@gfe.ufsb.edu.br

Tailisi Hoppe Trevizani
tailisi@usp.br

Paulo Alves de Lima Ferreira
paulo.alves.ferreira@hotmail.com

Cleverson Guizan Silva
cguizan@id.uff.br

Antônio Tadeu dos Reis
tadeu.reis@gmail.com

Denise Terroso
laraterroso@ua.pt

Layla Cristine da Silva
laylageologiauerj@gmail.com

Sergio Bergamaschi
sergioberg7@hotmail.com

Fernando Rocha
tavares.rocha@ua.pt

Monica Heilbron
monica.heilbron@gmail.com

- 1 Faculdade de Geologia, Universidade do Estado do Rio de Janeiro, UERJ, Av. São Francisco Xavier, 24, Sala 2020A, Maracanã, Rio de Janeiro, RJ 20550-013, Brazil
- 2 Departamento de Geociências, Universidade de Aveiro, GeoBioTec, Campus de Santiago, 3810-193 Aveiro, Portugal
- 3 Faculdade de Oceanografia, Universidade do Estado do Rio de Janeiro, UERJ, Rua São Francisco Xavier, 524, 4º Andar, Bloco E, Sala 4018, Rio de Janeiro, RJ 20550-900, Brazil
- 4 Instituto Oceanográfico, Universidade de São Paulo (IOUSP), Pça. do Oceanográfico, 191, Butantã, São Paulo 05508-120, Brazil
- 5 Centro de Formação em Ciências Ambientais (CFCam), Universidade Federal do Sul da Bahia (UFSB), Campus Sosígenes Costa, Rodovia Porto Seguro, Eunápolis, BR-367, km 10, Porto Seguro, Brazil
- 6 Instituto de Geociências, Universidade Federal Fluminense-UFF, Av. Milton Tavares de Souza, Boa Viagem, Niterói, RJ, Brazil